

1. Selection of soil moisture and SWE products

To our knowledge, there has not been a comprehensive evaluation of soil moisture and *SWE* datasets over Chile. Therefore, we included four different soil moisture datasets to calculate the ESSMI and two to calculate the SWEI to account for their uncertainty. Specifically, we used ERA5 (Hersbach et al., 2020),
5 ERA5-Land (Muñoz-Sabater et al., 2021), SMAP-L3E (O'Neill et al., 2016), and SMAP-L4SM (Reichle et al., 2018) to compute the ESSMI at different scales (1, 3, 6, and 12 months) and ERA5 and ERA5-Land to compute the SWEI (at 1, 3, and 6 months).

ERA5 (Hersbach et al., 2020) is an hourly reanalysis product that provides estimates of P , soil moisture at different depths (0–7, 7–28, 28–100, and 100–289 cm), and *SWE*, as well as other variables, from 1940
10 to the present with a spatial resolution of 0.25° . This product has a better representation of rain and snow than its predecessor, ERA-Interim, with a more realistic parameterisation of microphysics and mixed-phase clouds (Hersbach et al., 2020). Although ERA5 has a relatively coarse spatial resolution compared to other products, we included it in the analysis because reanalysis products tend to outperform purely observational datasets in high latitudes (Beck et al., 2017; Baez-Villanueva et al., 2021). The soil moisture depth used in
15 this study is 0–7 cm for consistency with the other soil moisture products.

The National Aeronautics and Space Administration (NASA) Soil Moisture Active Passive (SMAP) mission originally aimed to provide global measurements of soil moisture and freeze/thaw state using an L-band (active) radar and an L-band (passive) radiometer (Entekhabi et al., 2010). After the failure of the radar in early 2015, the radiometer remained as the only on-board sensor providing measurements (Chan et al.,
20 2016). The SMAP mission incorporated radio frequency interference detection and mitigation to provide more continuous high-quality estimates of soil moisture (Oliva et al., 2012; Mohammed et al., 2016). The observed radiometric brightness T comes from the land surface L-band emission, and is thus determined by the physical T and dielectric constant of the respective scene, which is related to soil moisture in the top ~ 5 cm surface soil moisture (Entekhabi et al., 2014).

25 The enhanced level-3 SMAP soil moisture product (SMAP-L3E; Entekhabi et al., 2010; O'Neill et al., 2016) provides global daily estimates of soil moisture derived from the SMAP level-1C interpolated brightness T with a 2–3 day average revisiting time. The SMAP level-4 soil moisture product (SMAP-L4SM; Entekhabi et al., 2010; Reichle et al., 2018) assimilates brightness T observations into the Goddard Earth Observing System (GEOS) Catchment land surface model. It has been validated against numerous ground-based measurements (Tavakol et al., 2019; Beck et al., 2021) and provides global 3-hourly volumetric soil moisture estimates of the top 5 cm.

30 To select a specific soil moisture and *SWE* product, we performed a simple correlation analysis between these indices at their respective temporal scales and the SSI-1. The selection of the products (one for each variable) was made considering the highest correlation and longest time series of the products, as we aim to
35 assess the ability of these indices to serve as a proxy for streamflow droughts. The selection of these products was based on the assumption that the product with the highest correlation with the SSI-1 represents better the spatio-temporal patterns of each variable across Chile. This assumption is not too far from reality since *i*) a correlation between different components of the water cycle at the monthly scale could indicate agreement

40 between the gridded products and in-situ Q data, and *ii*) any systematic bias that the products may present
do not affect the computation of the standardised drought indices.

Table S1 shows the cross-correlation values for all indices and the SSI-1. For the case of soil moisture, SMAP-L4SM has slightly better overall median cross-correlation values between ESSMI and SSI-1 (0.51), while ERA5 and ERA5 Land closely follow SMAP-L4SM (both products with a value of 0.50). However, ERA5 Land was selected as the best soil moisture product to compute the ESSMI drought index because
45 *i*) SMAP-L4SM is only available from 2015, which is much than the 32 years of record of ERA5-Land (although its evaluation starts in 1983) instead of gaining 0.01 in the cross-correlation evaluation, and *ii*) although ERA5 performed similarly to ERA5-Land, the latter has a higher spatial resolution.

In the case of SWEI, ERA5-Land was selected because it had the highest overall cross-correlation values compared to ERA5, and was therefore used to calculate the ESSMI and SWEI in the manuscript. Although
50 Muñoz-Sabater et al. (2021) found mixed performance of ERA5 Land related to SWE for some geographical locations and altitudes of the world, the product presents coherent SWE fields over continental Chile, which are very similar to those of ERA5.

Table S1. Median correlation values between the ESSMI and SWEI, and the SSI-1 over the 100 near-natural catchments presented in Figure 1 of the manuscript for 1979–2020.

Index	Product	Pearson's correlation coefficient
ESSMI	ERA5	Scale 1 (0.50); Scale 3 (0.49); Scale 6 (0.42); Scale 12 (0.30)
	ERA5-Land	Scale 1 (0.50); Scale 3 (0.47); Scale 6 (0.42); Scale 12 (0.29)
	SMAP-L3E	Scale 1 (0.34); Scale 3 (0.36); Scale 6 (0.26); Scale 12 (0.17)
	SMAP-L4SM	Scale 1 (0.51); Scale 3 (0.39); Scale 6 (0.27); Scale 12 (0.07)
SWEI	ERA5	Scale 1 (0.20); Scale 3 (0.21); Scale 6 (0.24)
	ERA5-Land	Scale 1 (0.23); Scale 3 (0.21); Scale 6 (0.22)

2. Conceptual figure of hydrological regimes

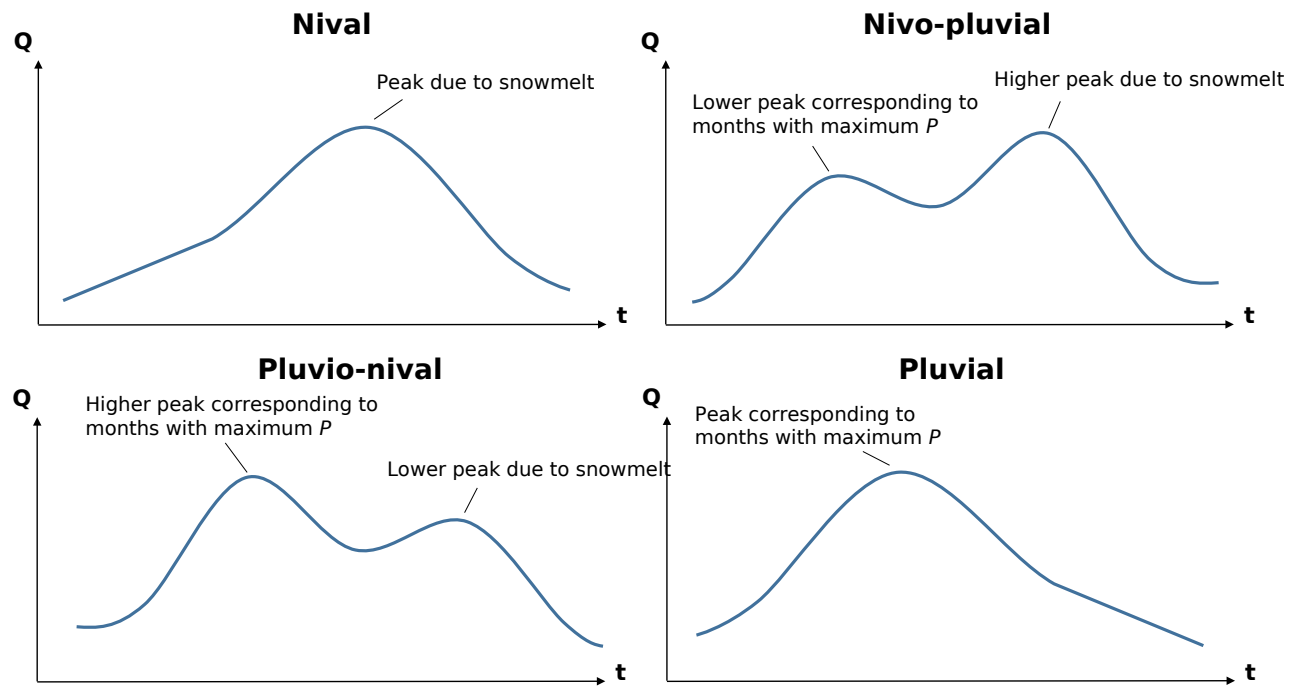


Figure S1. Conceptual illustration of the hydrological regimes used to classify the 100 near-natural catchments used in this study extracted from Baez-Villanueva et al. (2021).

3. Summary of scales with highest cross-correlation and event coincidence rates

Table S2. Median correlation (lag zero) and event coincidence rates for the selected indices and temporal scales with the highest values when calculated over 100 near-natural Chilean catchments.

Index	Temporal scale	Cross-correlation	Event coincidence	
			thr=1.0	thr=-1.5
SPI	3	0.57	0.52	
	6	0.58	0.53	0.46
	9	0.57	0.50	0.45
SPEI	3	0.52	0.50	
	6	0.52	0.51	0.41
	9		0.50	0.40
ESSMI	1	0.50	0.27	
	3	0.47	0.31	0.18
	6		0.29	0.21
SWEI	1	0.23	0.27	
	3		0.29	0.10
	6	0.22	0.29	0.08

Table S3. Temporal scale with the highest median correlation values (lag zero) for SPI, SPEI, ESSMI and SWEI calculated over 100 near-natural Chilean catchments. The number presented in parenthesis indicates the numeric value of the linear cross-correlation at the given temporal scale.

	Nival	Nivo-pluvial	Pluvio-Nival	Pluvial
SPI	12 (0.75)	12 (0.52)	3 (0.73)	3 (0.66)
	18 (0.75)	6 (0.51)	6 (0.79)	1 (0.53)
	24 (0.73)	3 (0.51)		
		9 (0.48)		
SPEI	12 (0.58)	3 (0.48)	3 (0.68)	3 (0.63)
	18 (0.60)	6 (0.43)	1 (0.67)	1 (0.55)
	24 (0.59)	12 (0.43)	6 (0.66)	
		1 (0.38)		
		9 (0.36)		
ESSMI	6 (0.53)	3 (0.49)	1 (0.55)	1 (0.52)
	3 (0.48)	1 (0.48)	3 (0.50)	
	1 (0.38)			
SWEI	1 (0.38)	1 (0.25)	1 (0.25)	3 (0.10)

Table S4. Temporal scale with the highest median precursory coincidence rates for SPI, SPEI, ESSMI and SWEI calculated over 100 near-natural Chilean catchments. Numbers in parentheses indicate the numeric value of the precursory coincidence rate at the given temporal scale. This table corresponds to moderate drought events ($thr = -1.0$).

	Nival	Nivo-pluvial	Pluvio-Nival	Pluvial
SPI	24 (0.74)	6 (0.48)	6 (0.68)	3 (0.55)
	18 (0.68)	9 (0.47)		
		12 (0.46)		
SPEI	18 (0.52)	9 (0.50)	3 (0.60)	3 (0.49)
		6 (0.49)	1 (0.55)	
		12 (0.45)		
ESSMI	1 (0.23)	1 (0.26)	3 (0.37)	6 (0.38)
	3 (0.22)			3 (0.37)
SWEI	-	-	-	-

Table S5. Temporal scale with the highest median precursory coincidence rates for SPI, SPEI, ESSMI and SWEI calculated over 100 near-natural Chilean catchments. Numbers in parentheses indicate the numeric value of the precursory coincidence rate at the given temporal scale. This table corresponds to severe drought events ($thr = -1.5$).

	Nival	Nivo-pluvial	Pluvio-Nival	Pluvial
SPI	24 (0.66)	6 (0.32)	6 (0.73)	-
		9 (0.31)		
		3 (0.31)		
SPEI	12 (0.25)	6 (0.32)	6 (0.48)	12 (0.30)
		9 (0.31)	3 (0.47)	
		12 (0.30)		
ESSMI	-	-	6 (0.25)	1 (0.23)
			3 (0.23)	3 (0.22)
SWEI	-	-	-	-

3 All catchments — Boxplots for different temporal scales and lag times

3.1 Cross-correlation

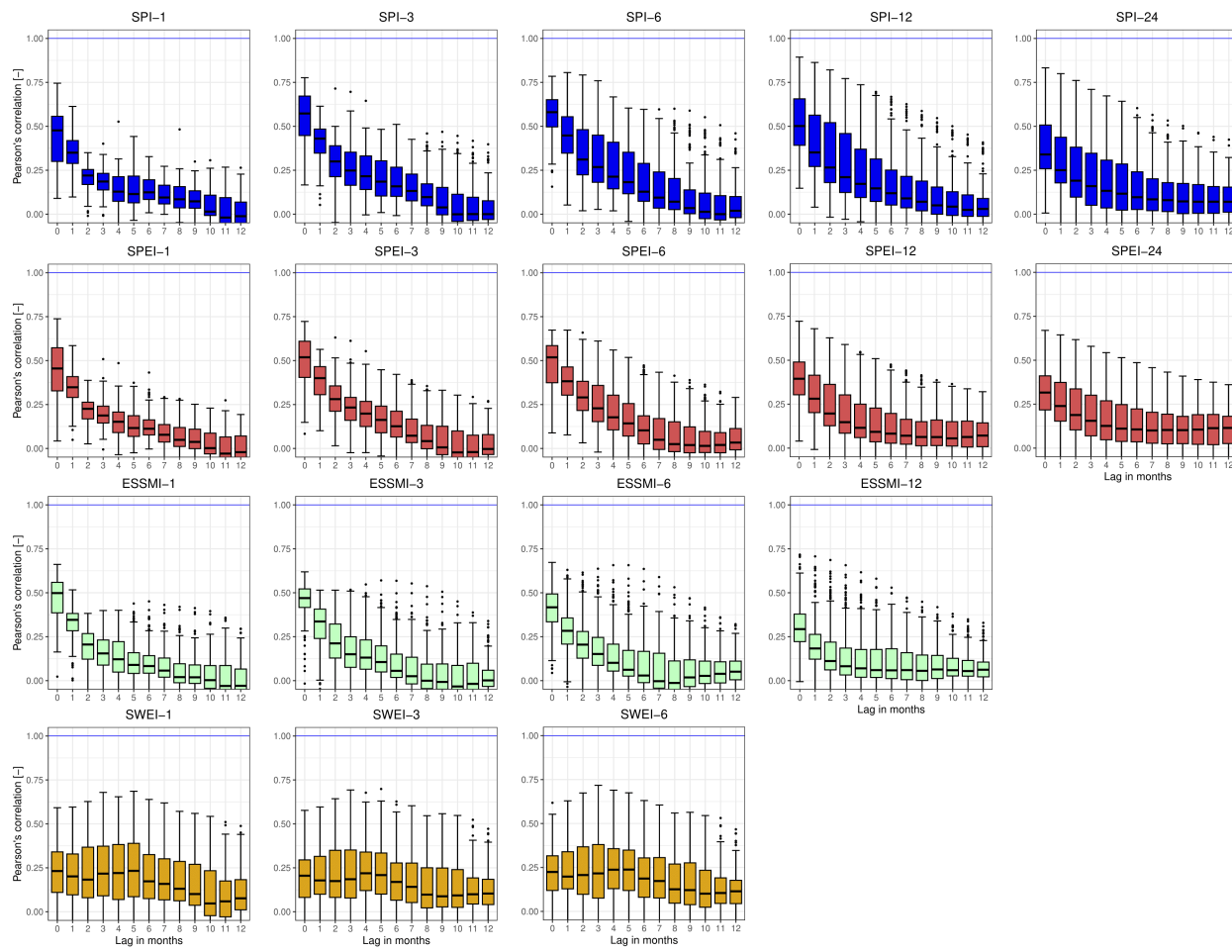


Figure S2. cross-correlation among the selected drought indices (SPI, SPEI, ESSMI, SWEI) and the SSI-1, for different temporal scales (from 1 to 24 months) and lag times (from 0 to 12 months). The solid coloured boxplots indicate lags where at least 75% of the catchments presented significant results at the 95% confidence interval, while the white boxplots indicate the opposite. The blue line indicates the optimal cross-correlation. The solid line within each box represents the median value, the edges of the boxes represent the first and third quartiles, and the whiskers extend to the most extreme data point which is no more than 1.5 times the interquartile range from the box.

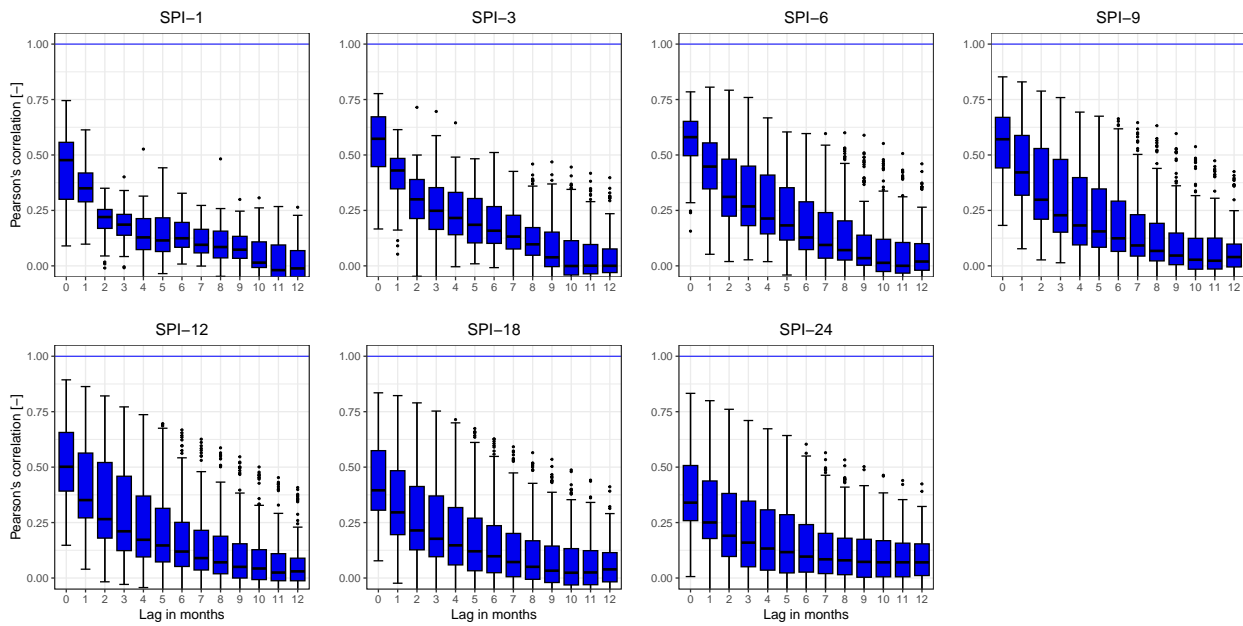


Figure S3. cross-correlation results between the SPI and the SSI-1 at different lag periods (ranging from 0 to 12 months). The blue line indicates the optimal cross-correlation. The solid line within each box represents the median value, the edges of the boxes represent the first and third quartiles, and the whiskers extend to the most extreme data point which is no more than 1.5 times the interquartile range from the box.

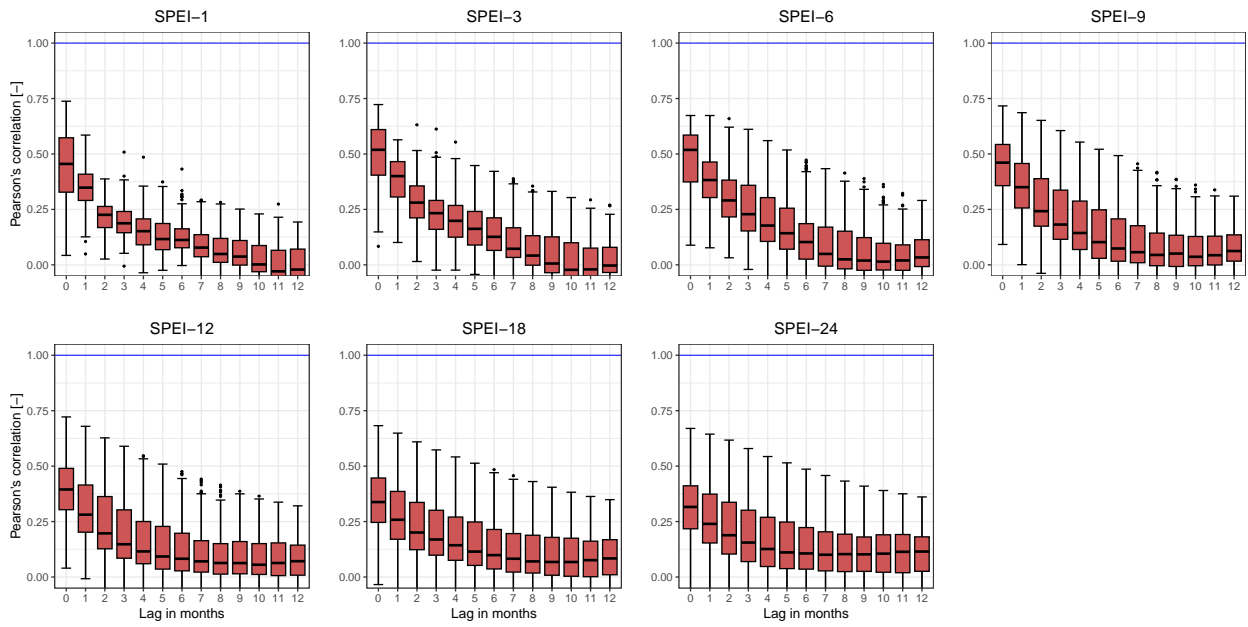


Figure S4. cross-correlation results between the SPEI and the SSI-1 at different lag periods (ranging from 0 to 12 months). The blue line indicates the optimal cross-correlation. The solid line within each box represents the median value, the edges of the boxes represent the first and third quartiles, and the whiskers extend to the most extreme data point which is no more than 1.5 times the interquartile range from the box.

3.2 Event coincidence analysis

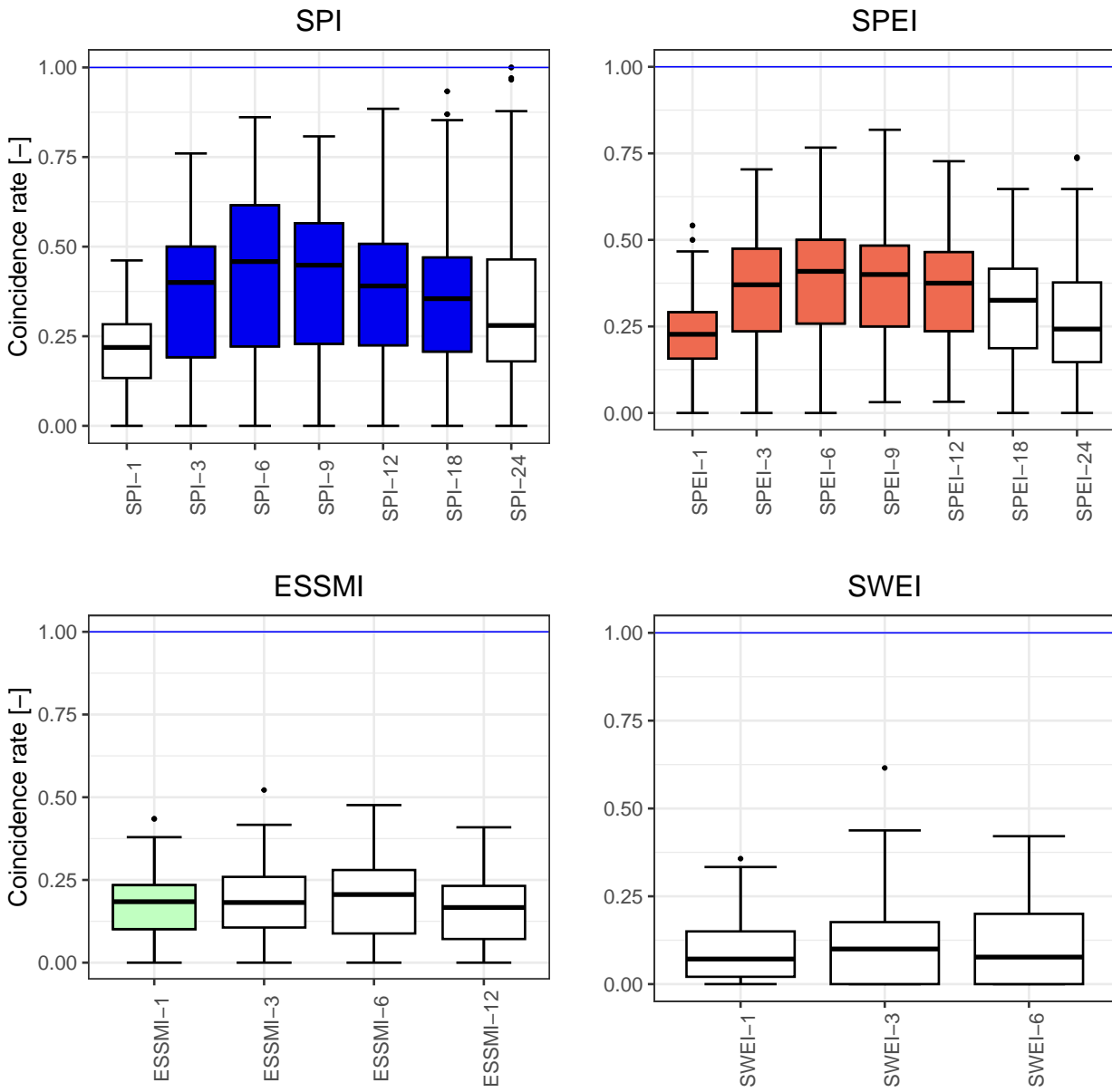


Figure S5. Event coincidence analysis results of the selected drought indices and the SSI-1 at a lag of zero months for severe droughts ($thr = -1.5$). The coloured boxplots indicate lags where at least 75% of the catchments presented significant results at the 95% confidence interval, while the white boxplots indicate the opposite. The blue line indicates the optimal cross-correlation. The solid line within each box represents the median value, the edges of the boxes represent the first and third quartiles, and the whiskers extend to the most extreme data point which is no more than 1.5 times the interquartile range from the box.

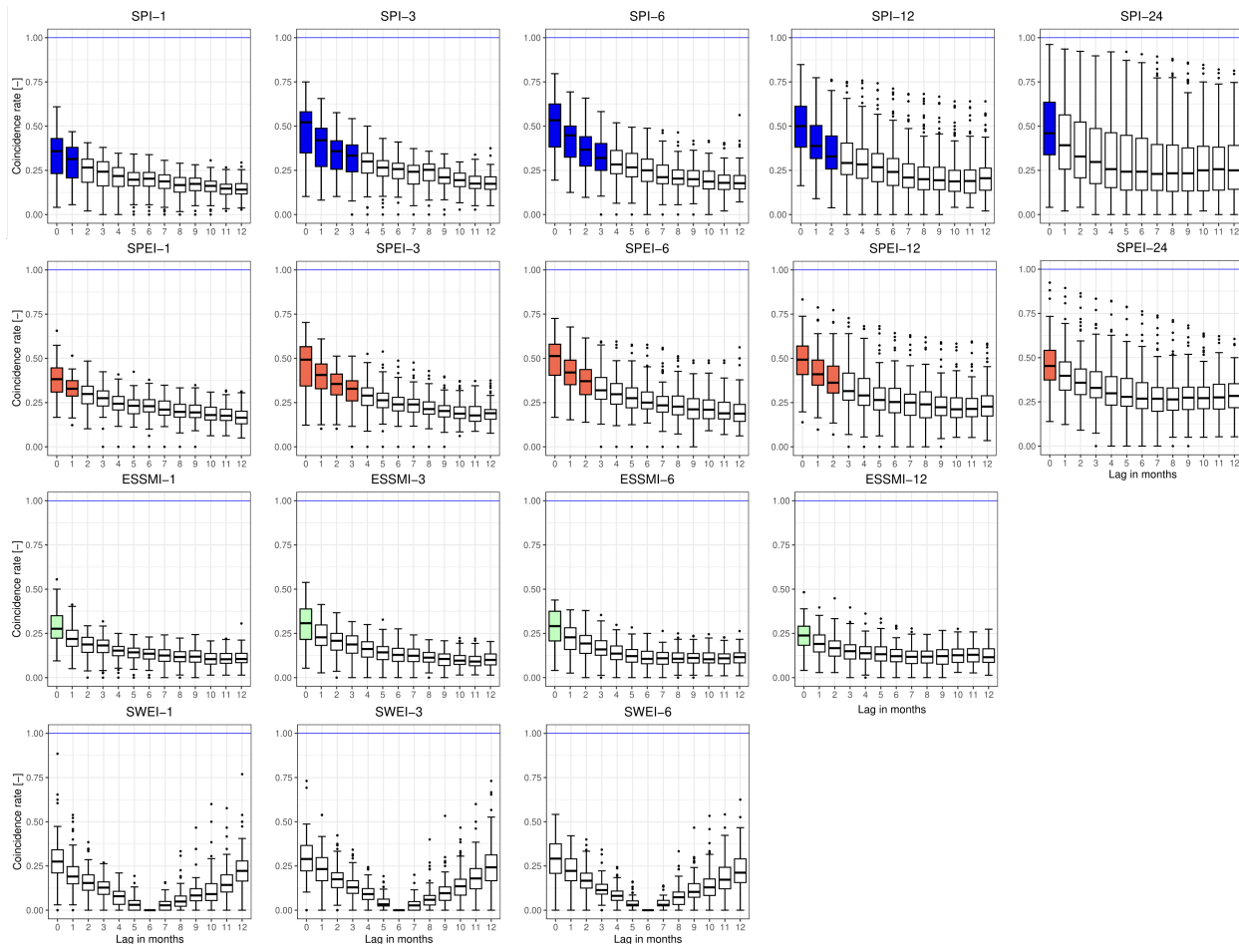


Figure S6. Event coincidence analysis results of the selected drought indices and the SSI-1 at different lag periods (ranging from 0 to 12 months) for a threshold of -1.0 (moderate droughts). The solid coloured boxplots indicate those lags where at least 75% of the catchments presented significant results at the 95% confidence interval, while the white boxplots indicate the opposite. The blue line indicates the optimal cross-correlation. The solid line within each box represents the median value, the edges of the boxes represent the first and third quartiles, and the whiskers extend to the most extreme data point which is no more than 1.5 times the interquartile range from the box.

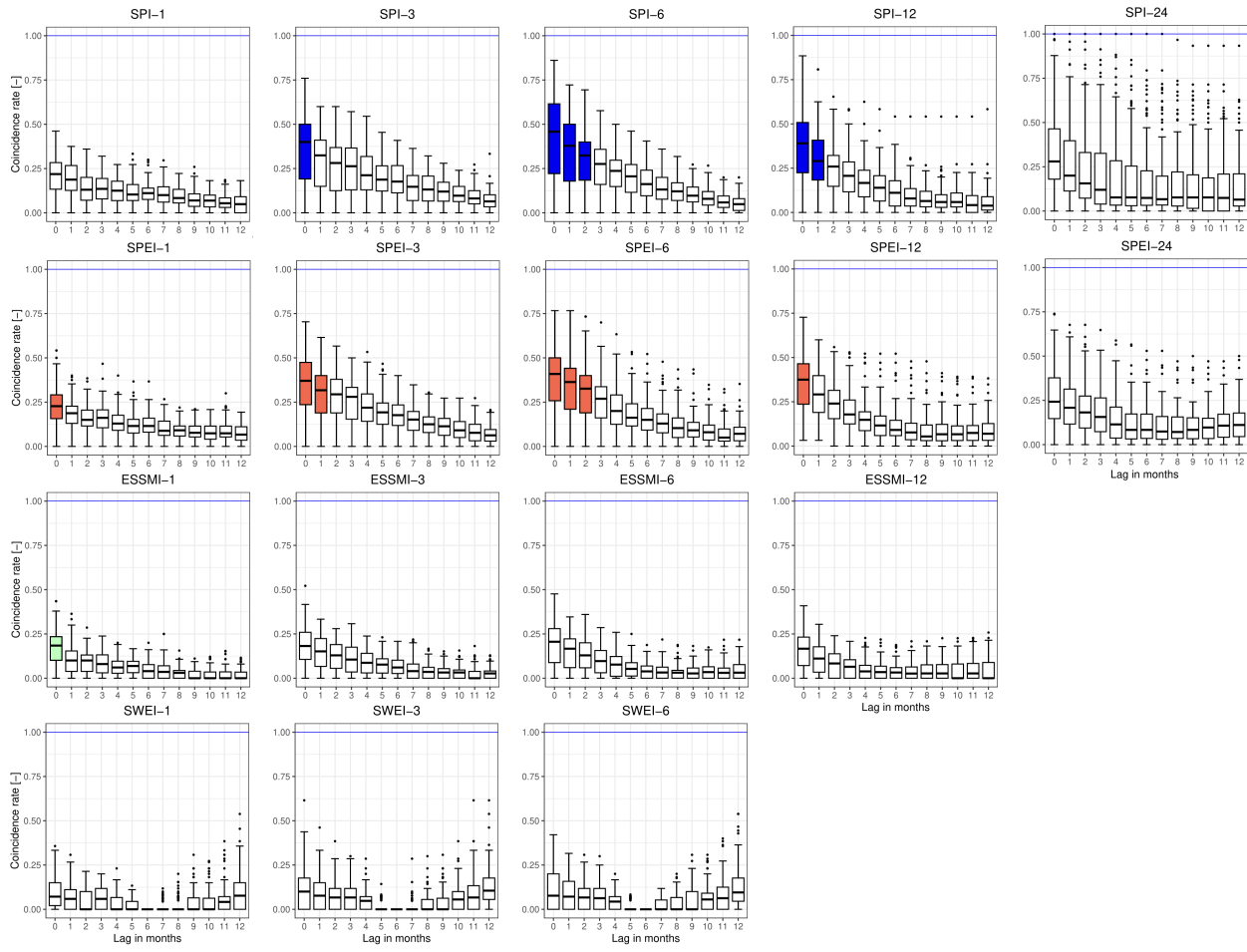


Figure S7. Event coincidence analysis results of the selected drought indices and the SSI-1 at different lag periods (ranging from 0 to 12 months) for a threshold of -1.5 (severe droughts). The solid coloured boxplots indicate those lags where at least 75% of the catchments presented significant results at the 95% confidence interval, while the white boxplots indicate the opposite. The blue line indicates the optimal cross-correlation. The solid line within each box represents the median value, the edges of the boxes represent the first and third quartiles, and the whiskers extend to the most extreme data point which is no more than 1.5 times the interquartile range from the box.

60 **4 All catchments — Spatial analysis for different temporal scales and lag times**

4.1 Cross-correlation

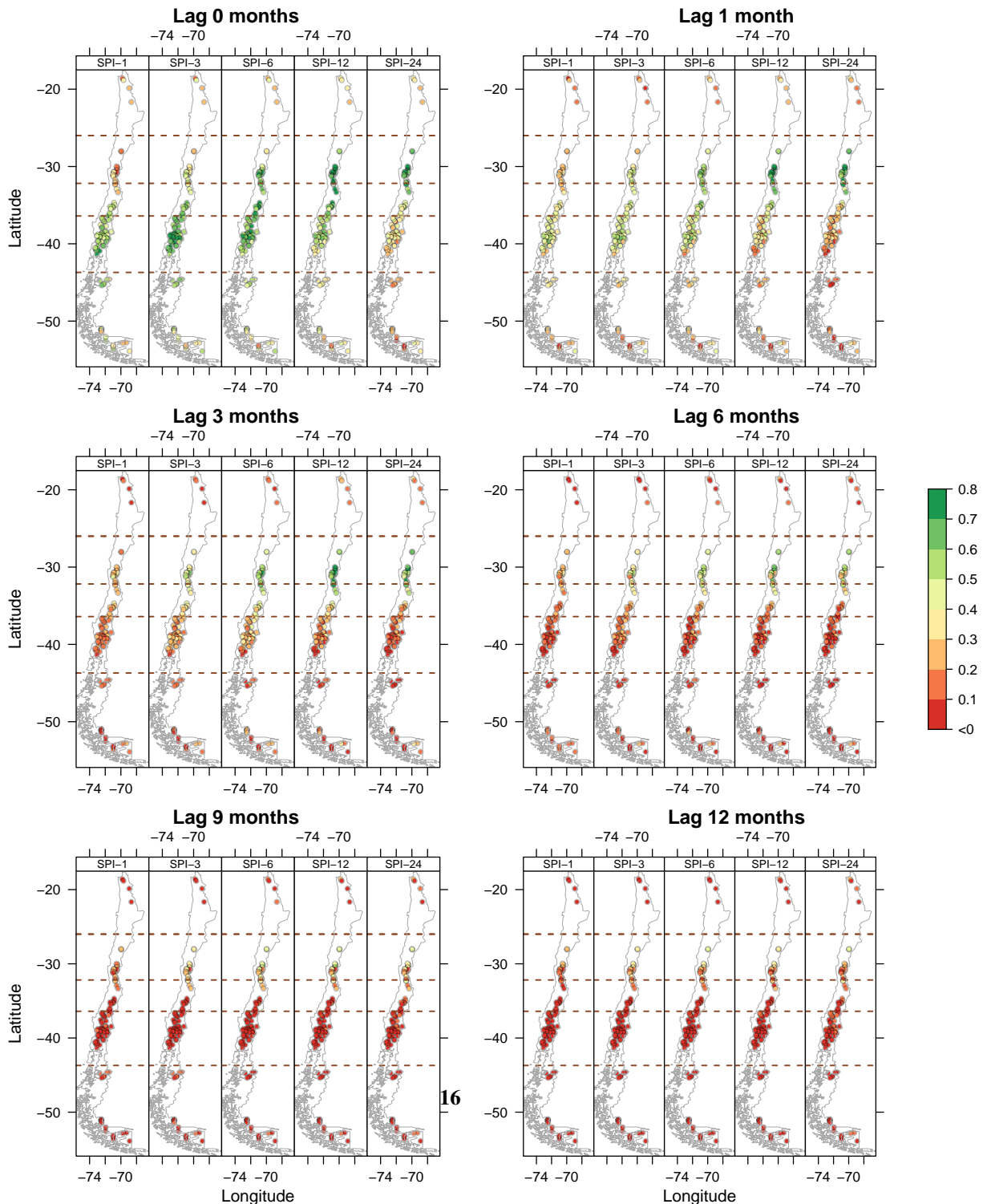


Figure S8. Spatial distribution of the cross-correlation results between the SPI at different scales and the SSI-1 over 100 near-natural catchments at different lags (0, 1, 3, 6, 9, and 12 months).

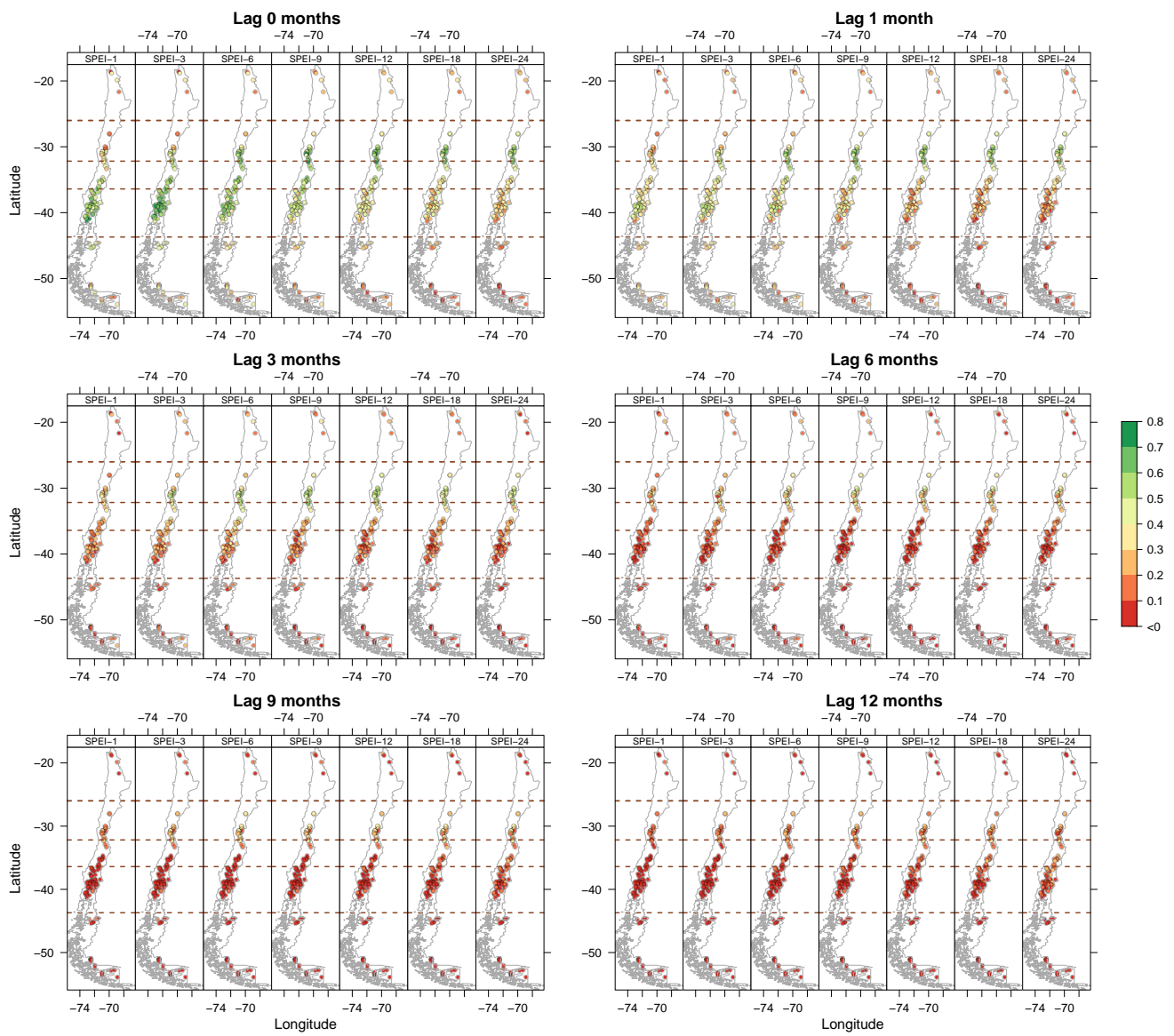


Figure S9. Spatial distribution of the cross-correlation results between the SPEI at different scales and the SSI-1 over 100 near-natural catchments at different lags (0, 1, 3, 6, 9, and 12 months).

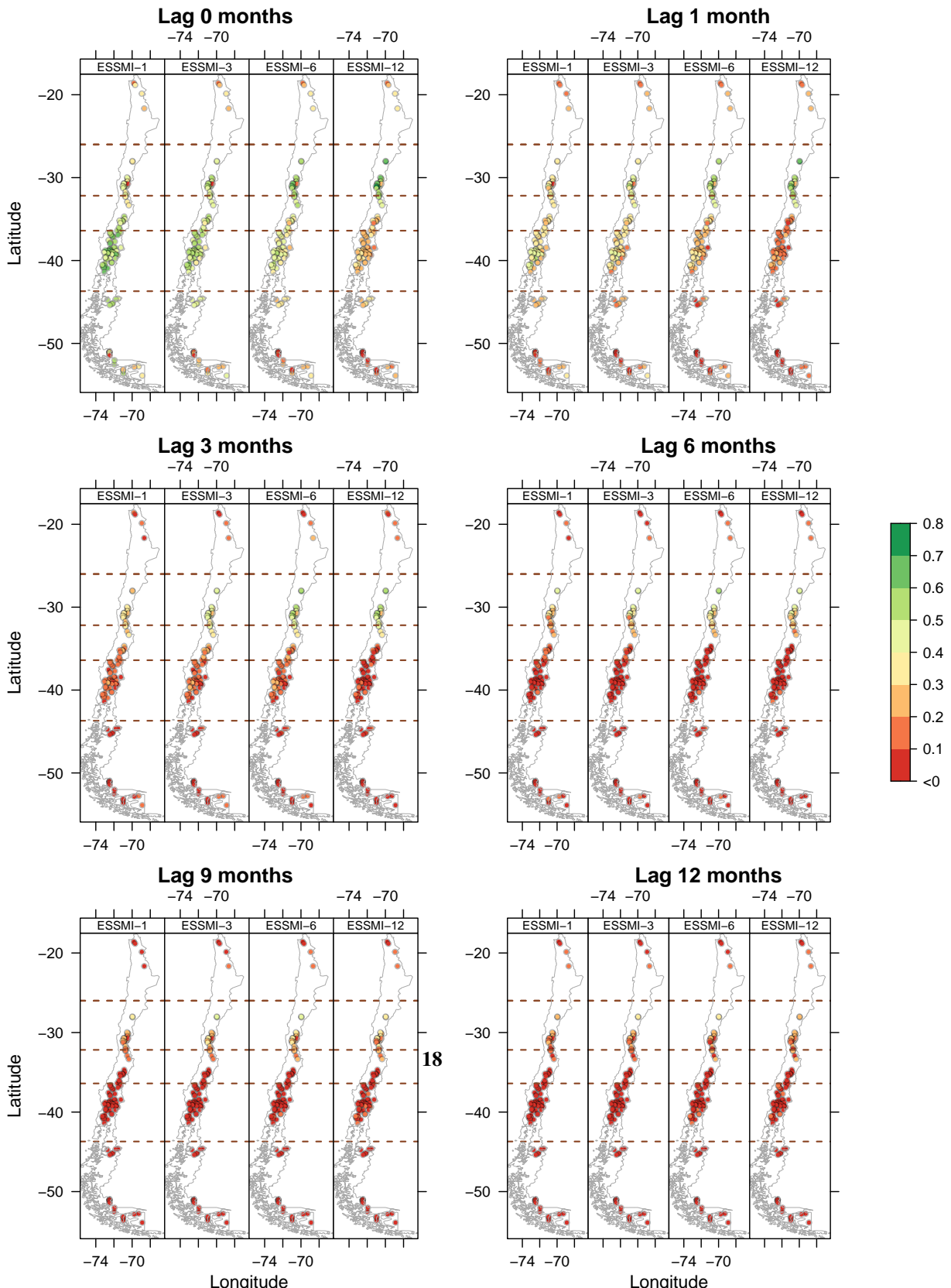


Figure S10. Spatial distribution of the cross-correlation results between the ESSMI at different scales and the SSI-1 over 100 near-natural catchments at different lags (0, 1, 3, 6, 9, and 12 months).

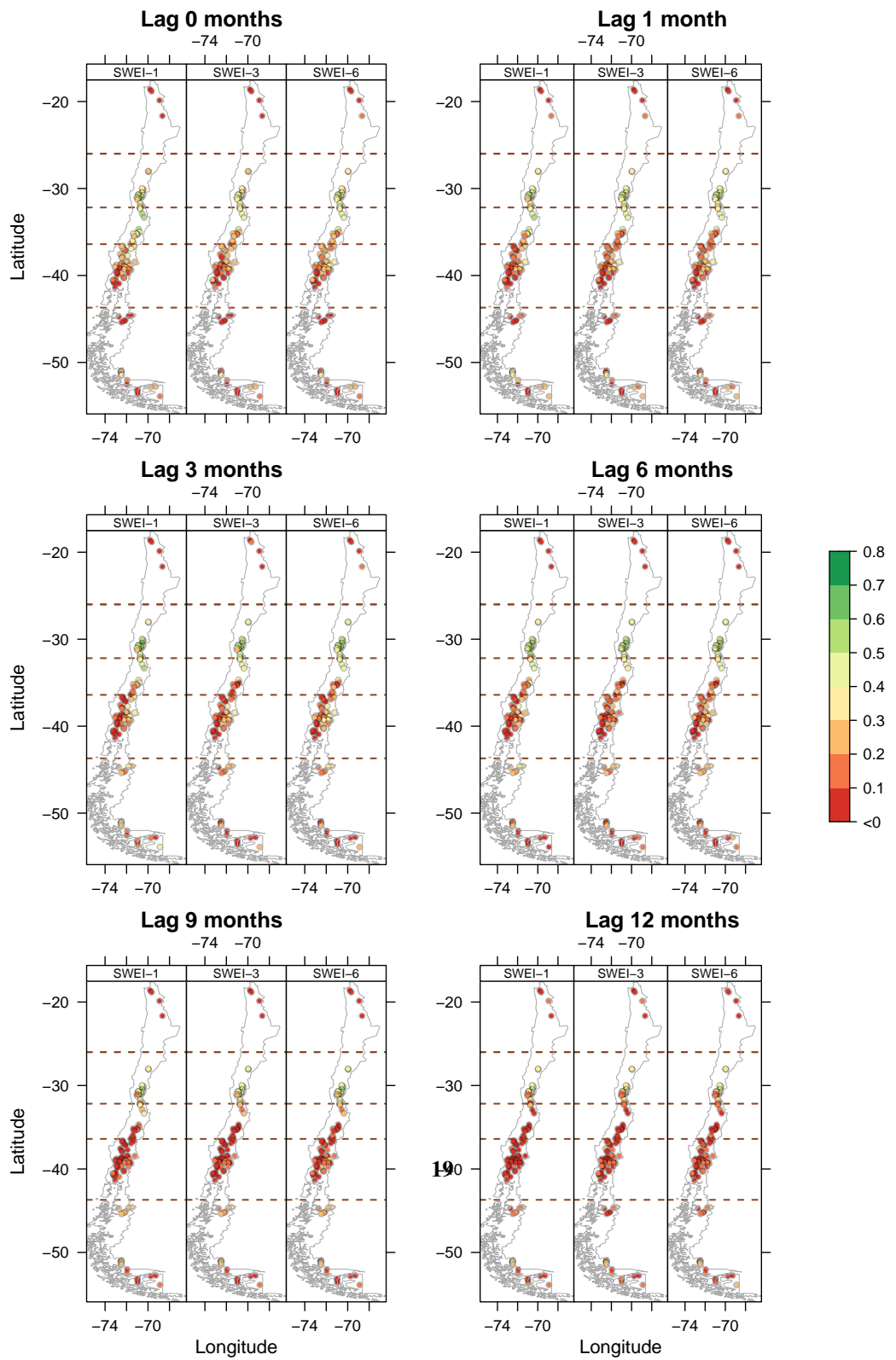


Figure S11. Spatial distribution of the cross-correlation results between the SWEI at different scales and the SSI-1 over 100 near-natural catchments at different lags (0, 1, 3, 6, 9, and 12 months).

4.2 Event coincidence analysis

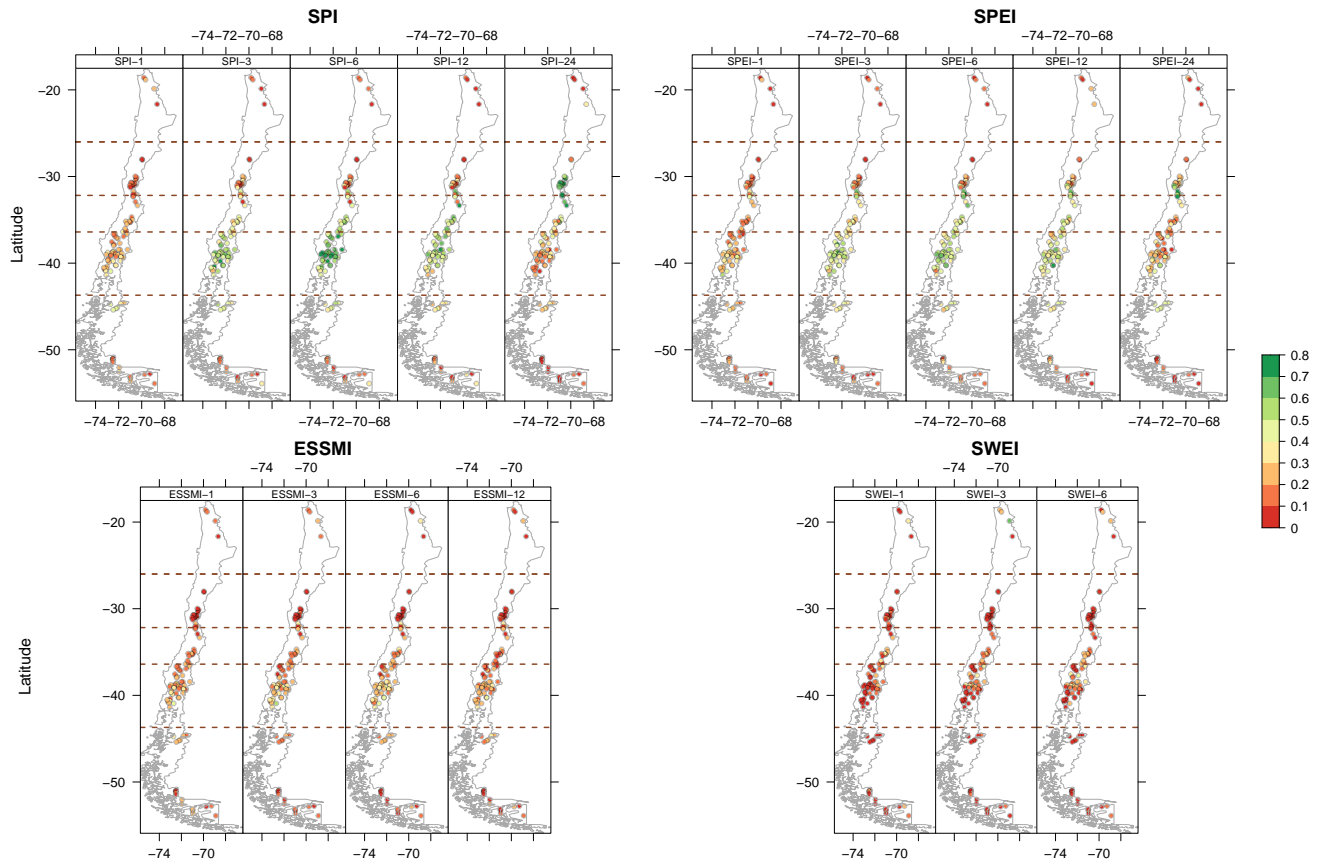


Figure S12. Spatial distribution of the event coincidence analysis results for severe droughts between the selected indices and the SSI-1 over 100 near-natural catchments and at a lag of zero months.

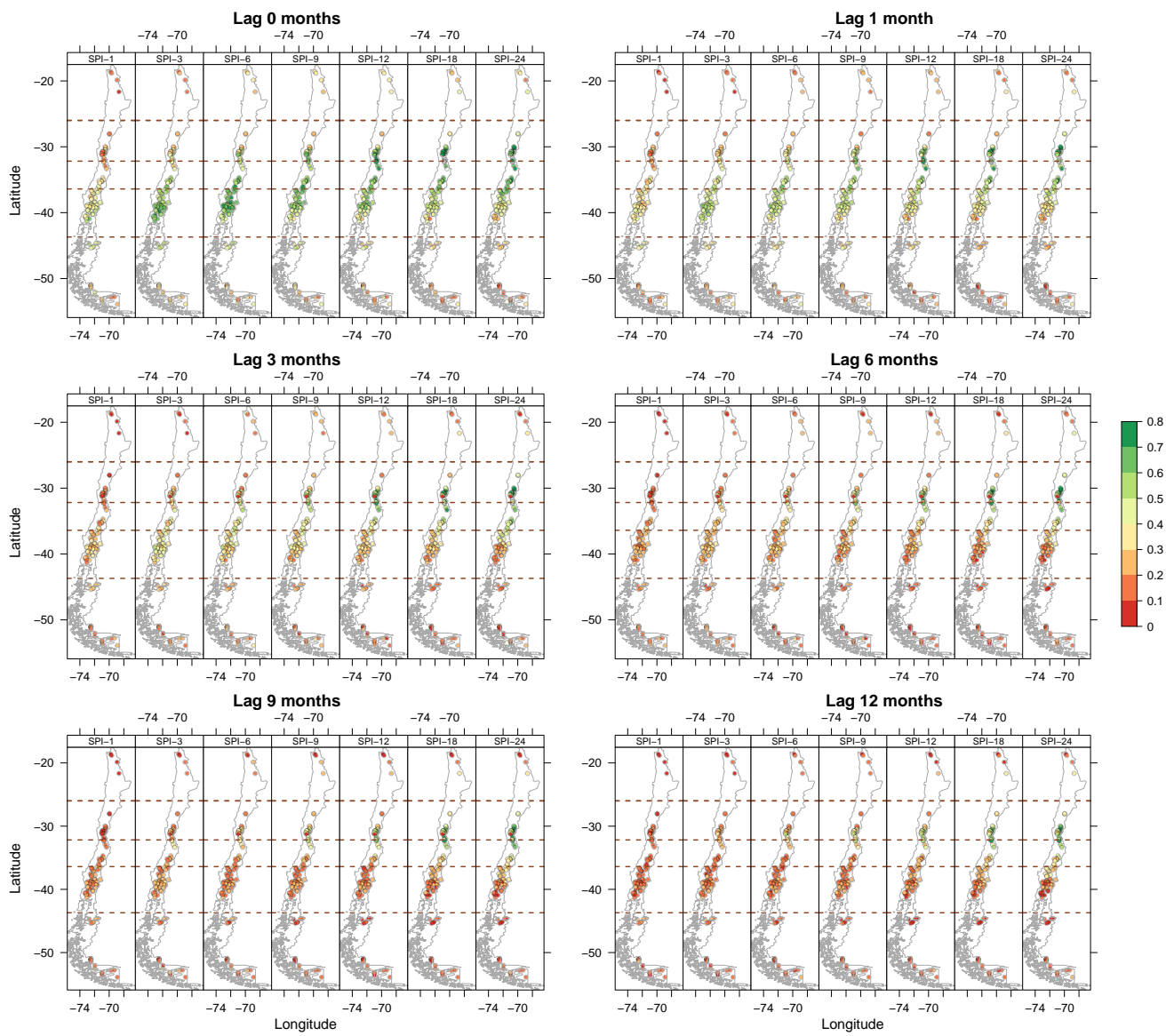


Figure S13. Spatial distribution of the event coincidence analysis results for moderate droughts between the SPI and the SSI-1 over 100 near-natural catchments and at different lags (0, 1, 3, 6, 9, and 12 months).

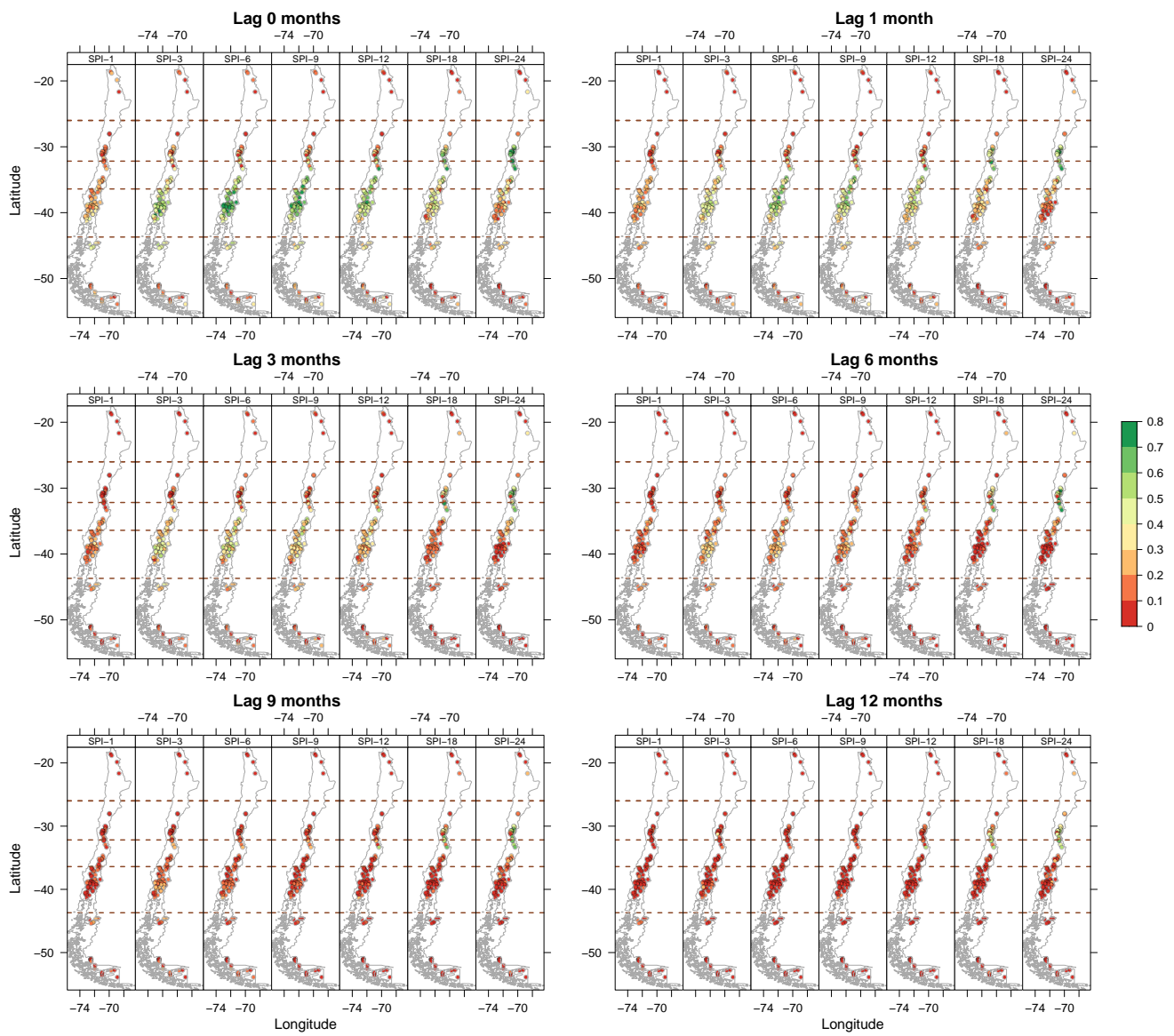


Figure S14. Spatial distribution of the event coincidence analysis results for severe droughts between the SPI and the SSI-1 over 100 near-natural catchments and at different lags (0, 1, 3, 6, 9, and 12 months).

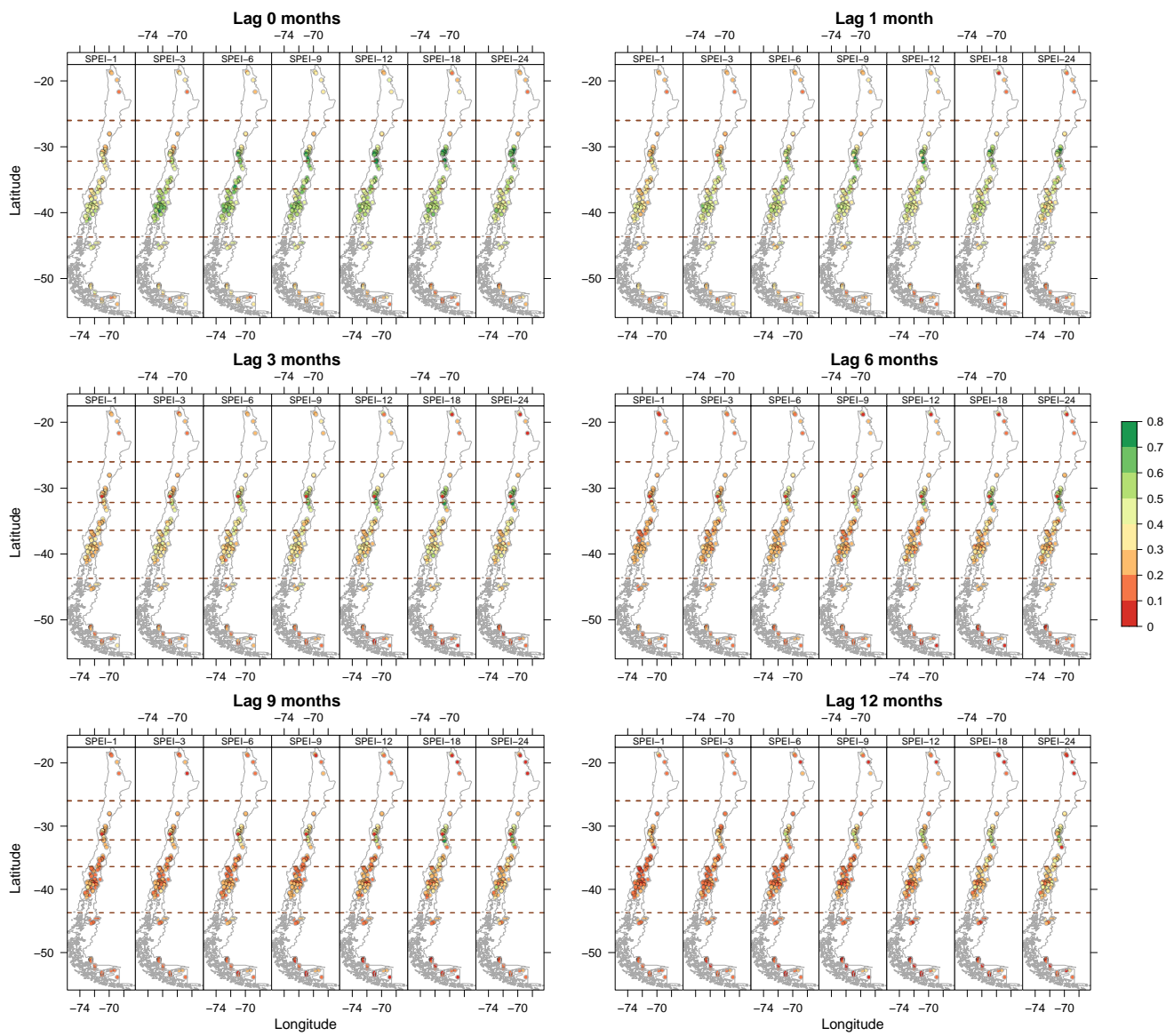


Figure S15. Spatial distribution of the event coincidence analysis results for moderate droughts between the SPEI and the SSI-1 over 100 near-natural catchments and at different lags (0, 1, 3, 6, 9, and 12 months).

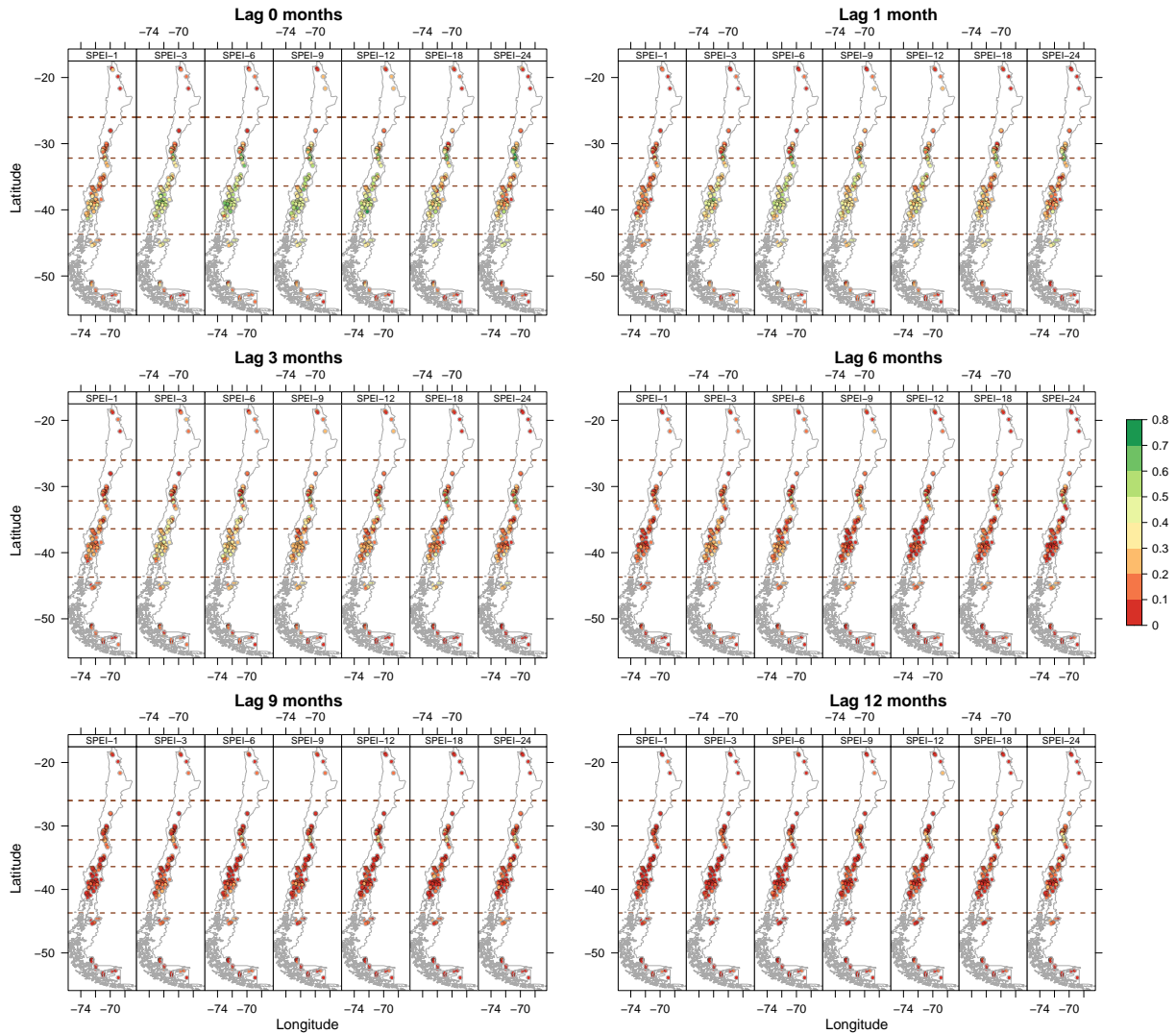


Figure S16. Spatial distribution of the event coincidence analysis results for severe droughts between the SPEI and the SSI-1 over 100 near-natural catchments and at different lags (0, 1, 3, 6, 9, and 12 months).

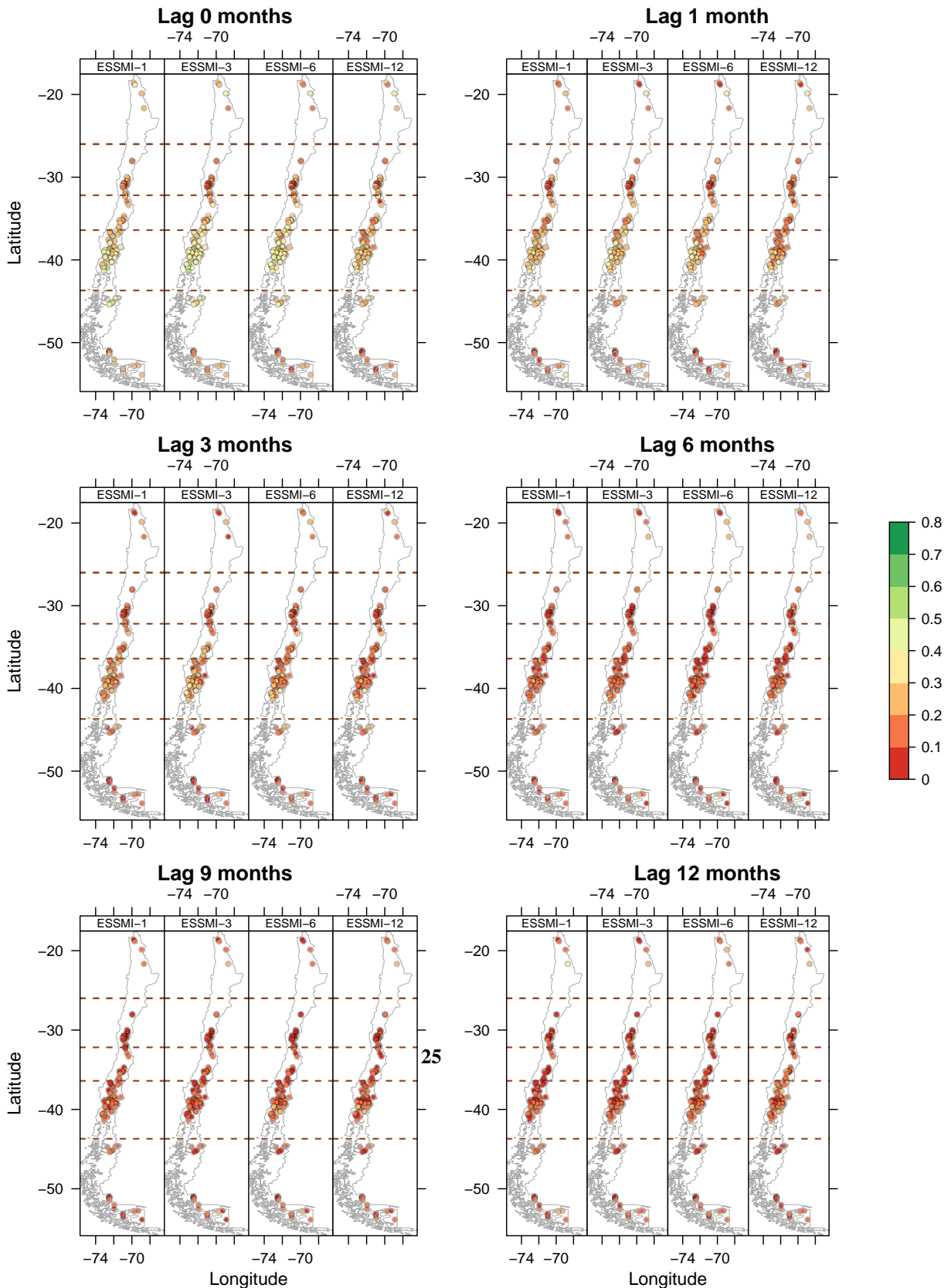


Figure S17. Spatial distribution of the event coincidence analysis results for severe droughts between the ESSMI and the SSI-1 over 100 near-natural catchments and at different lags (0, 1, 3, 6, 9, and 12 months).

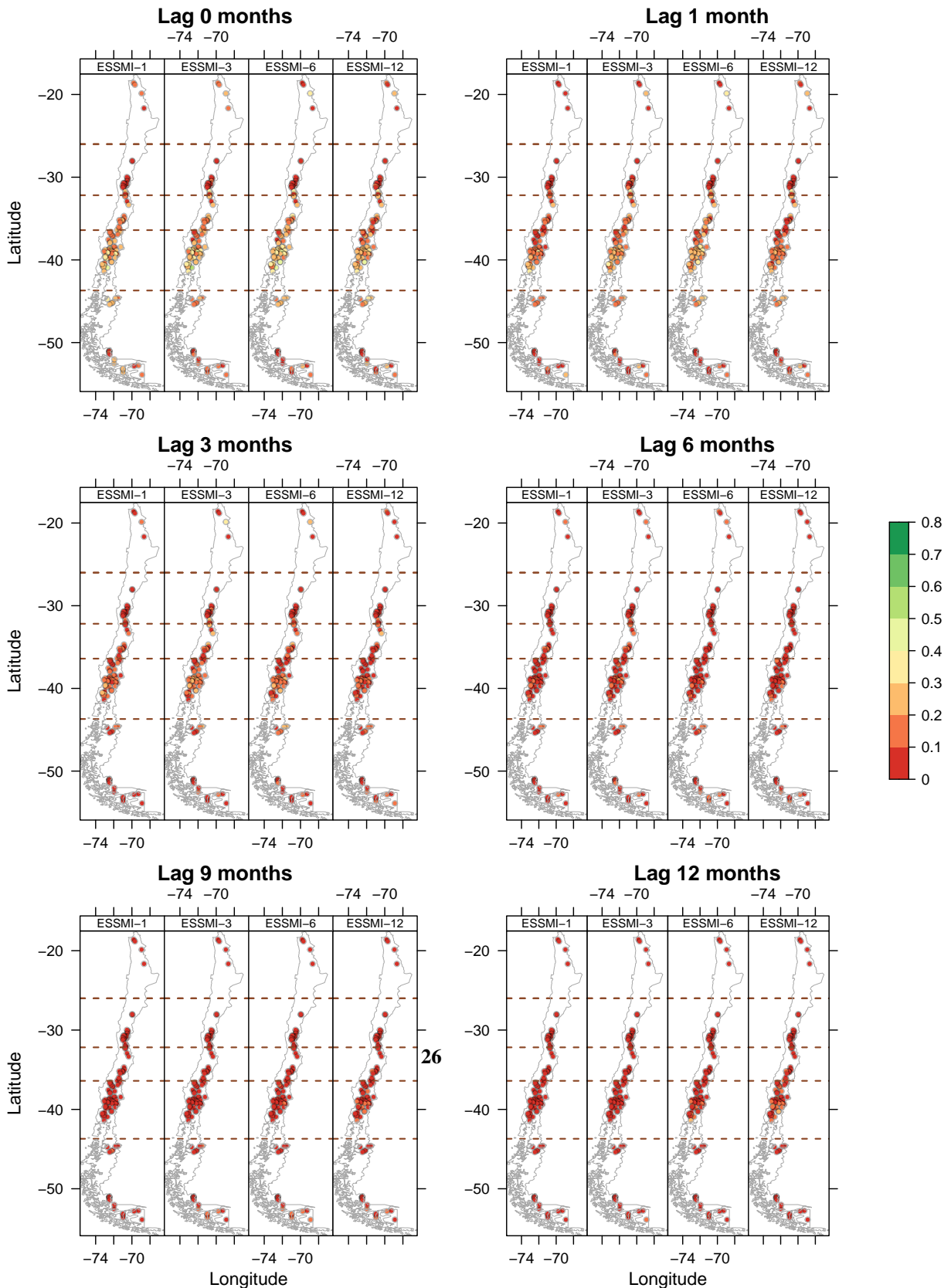


Figure S18. Spatial distribution of the event coincidence analysis results for severe droughts between the ESSMI and the SSI-1 over 100 near-natural catchments and at different lags (0, 1, 3, 6, 9, and 12 months).

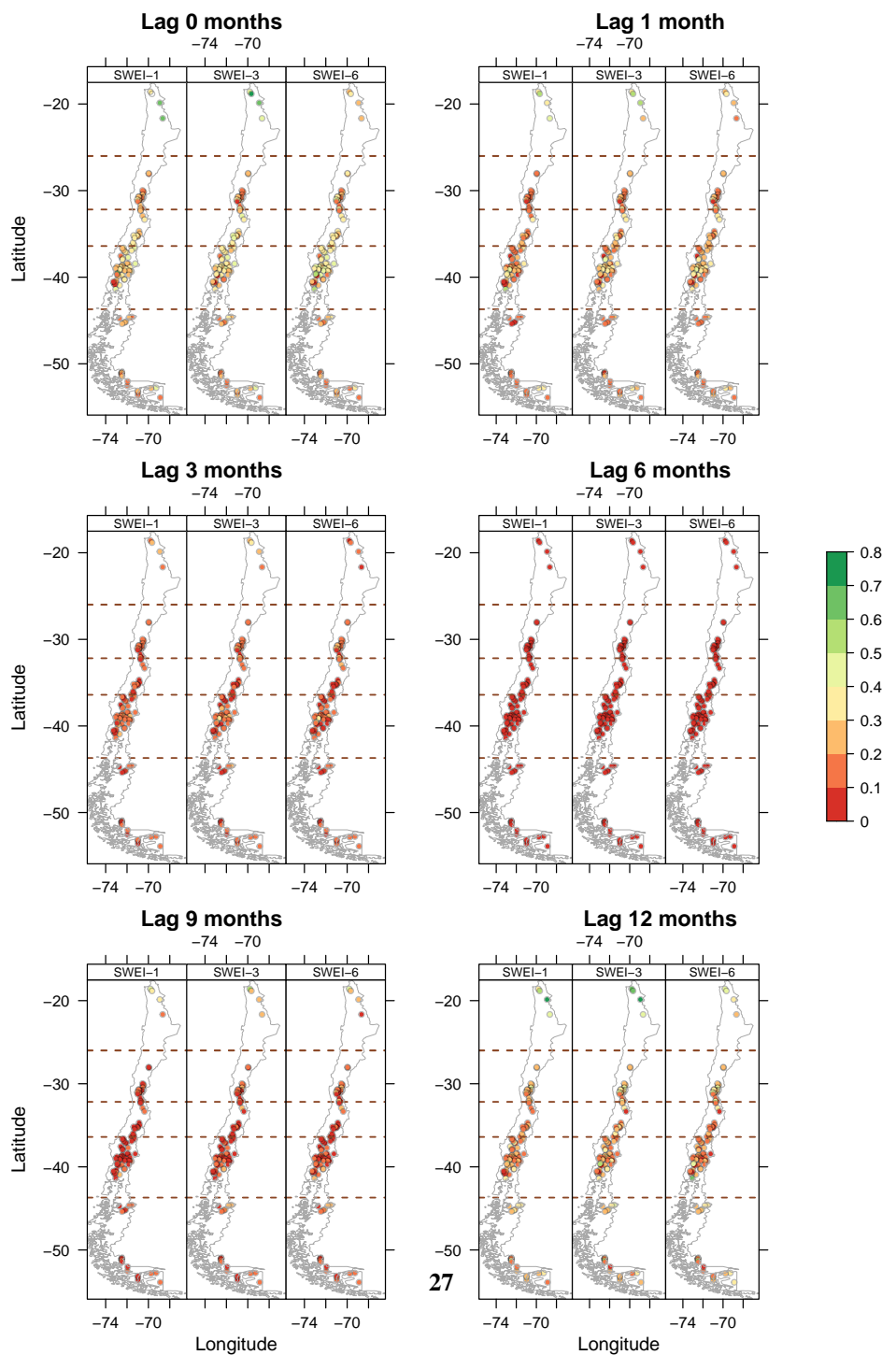


Figure S19. Spatial distribution of the event coincidence analysis results for moderate droughts between the SWEI and the SSI-1 over 100 near-natural catchments and at different lags (0, 1, 3, 6, 9, and 12 months).

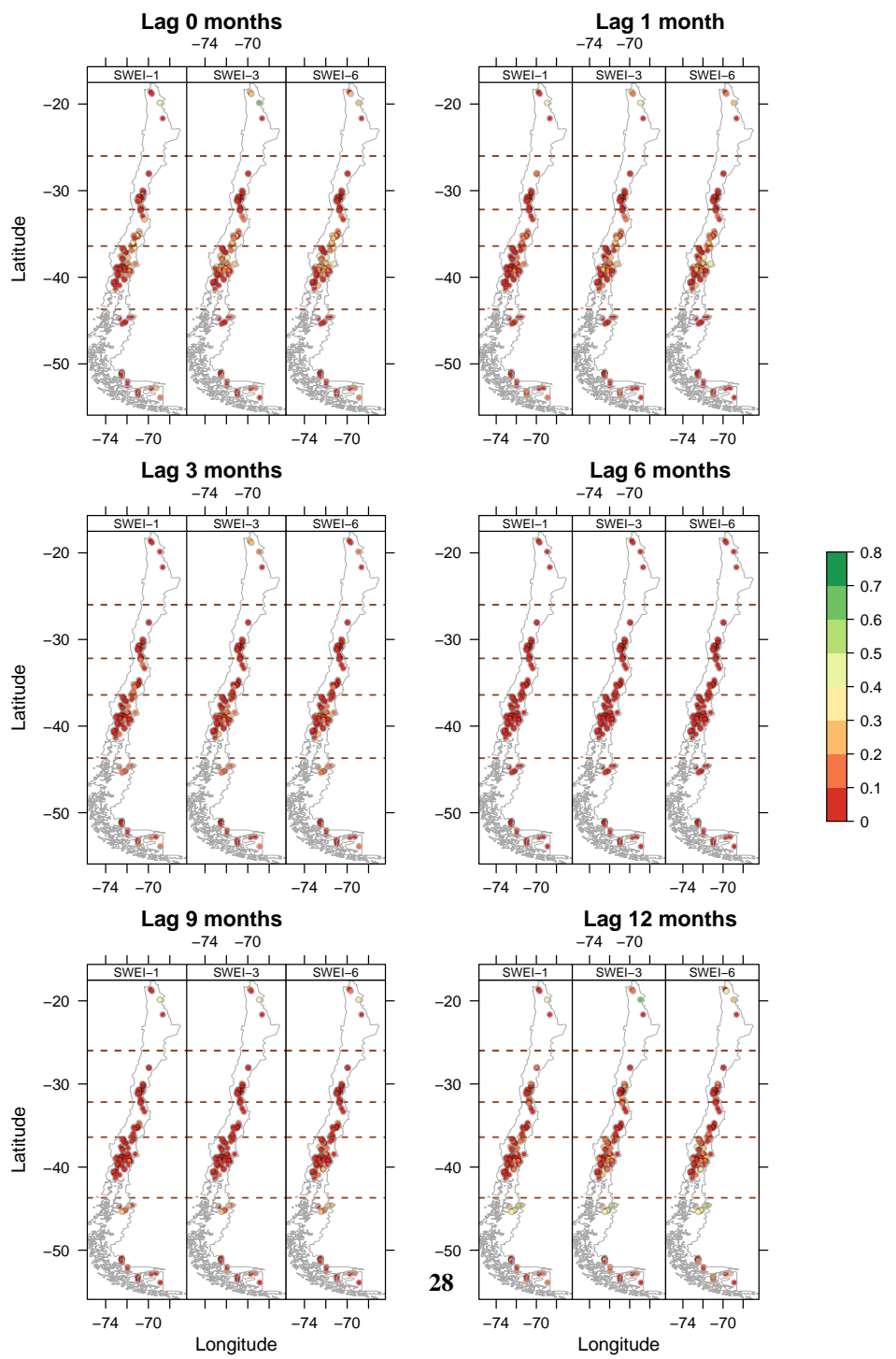


Figure S20. Spatial distribution of the event coincidence analysis results for severe droughts between the SWEI and the SSI-1 over 100 near-natural catchments and at different lags (0, 1, 3, 6, 9, and 12 months).

5. Cross-Correlation analysis – Hydrological Regimes

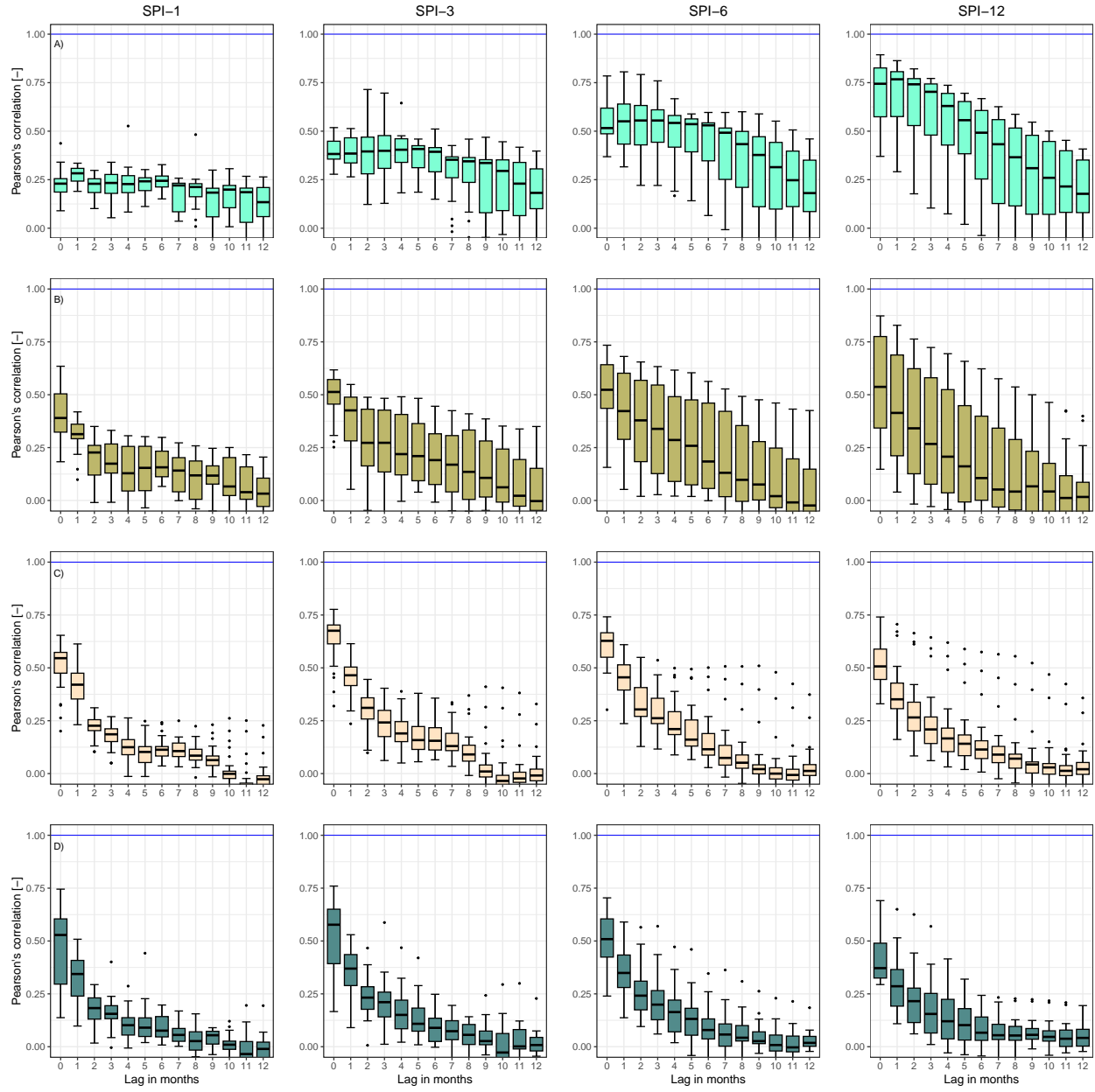


Figure S21. cross-correlation results of the SPI and the SSI-1 at different lag periods (ranging from 0 to 12 months) for *i*) snow-dominated catchments (a); *ii*) nivo-pluvial (b); *iii*) pluvio-nival (c); and *iv*) rain-dominated (d) catchments. The blue line indicates the optimal cross-correlation. The solid line within each box represents the median value, the edges of the boxes represent the first and third quartiles, and the whiskers extend to the most extreme data point which is no more than 1.5 times the interquartile range from the box.

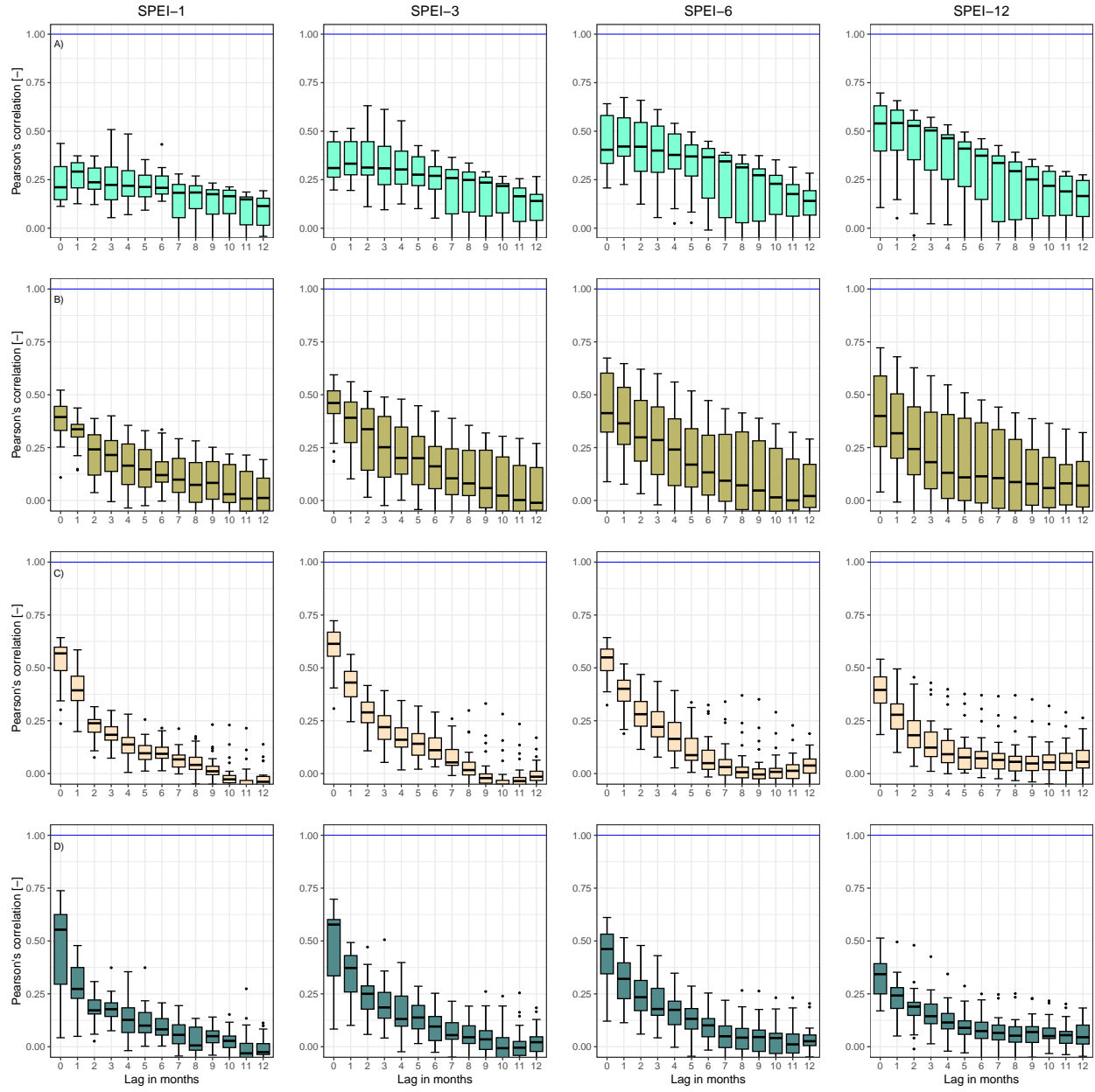


Figure S22. cross-correlation results of the SPEI and the SSI-1 at different lag periods (ranging from 0 to 12 months) for *i*) snow-dominated catchments (a); *ii*) nivo-pluvial (b); *iii*) pluvio-nival (c); and *iv*) rain-dominated (d) catchments. The blue line indicates the optimal cross-correlation. The solid line within each box represents the median value, the edges of the boxes represent the first and third quartiles, and the whiskers extend to the most extreme data point which is no more than 1.5 times the interquartile range from the box.

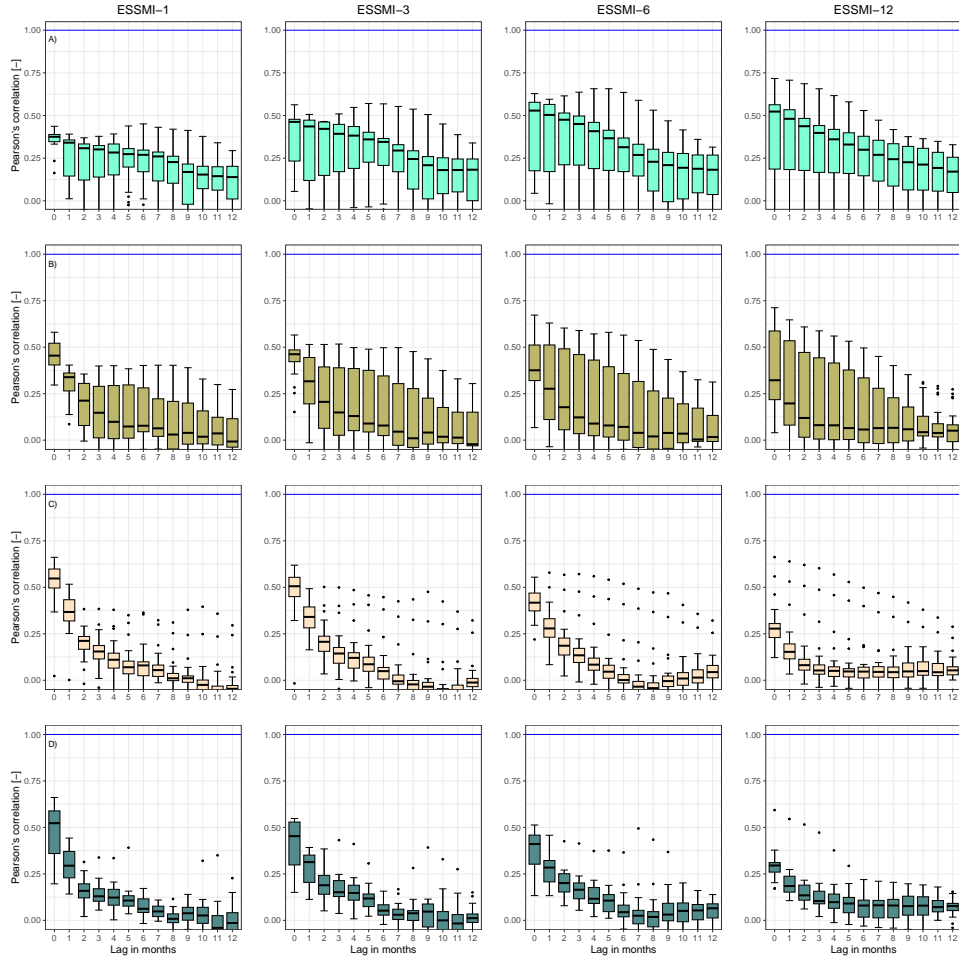


Figure S23. cross-correlation results of the ESSMI and the SSI-1 at different lag periods (ranging from 0 to 12 months) for *i*) snow-dominated catchments (a); *ii*) nivo-pluvial (b); *iii*) pluvio-nival (c); and *iv*) rain-dominated (d) catchments. The blue line indicates the optimal cross-correlation. The solid line within each box represents the median value, the edges of the boxes represent the first and third quartiles, and the whiskers extend to the most extreme data point which is no more than 1.5 times the interquartile range from the box.

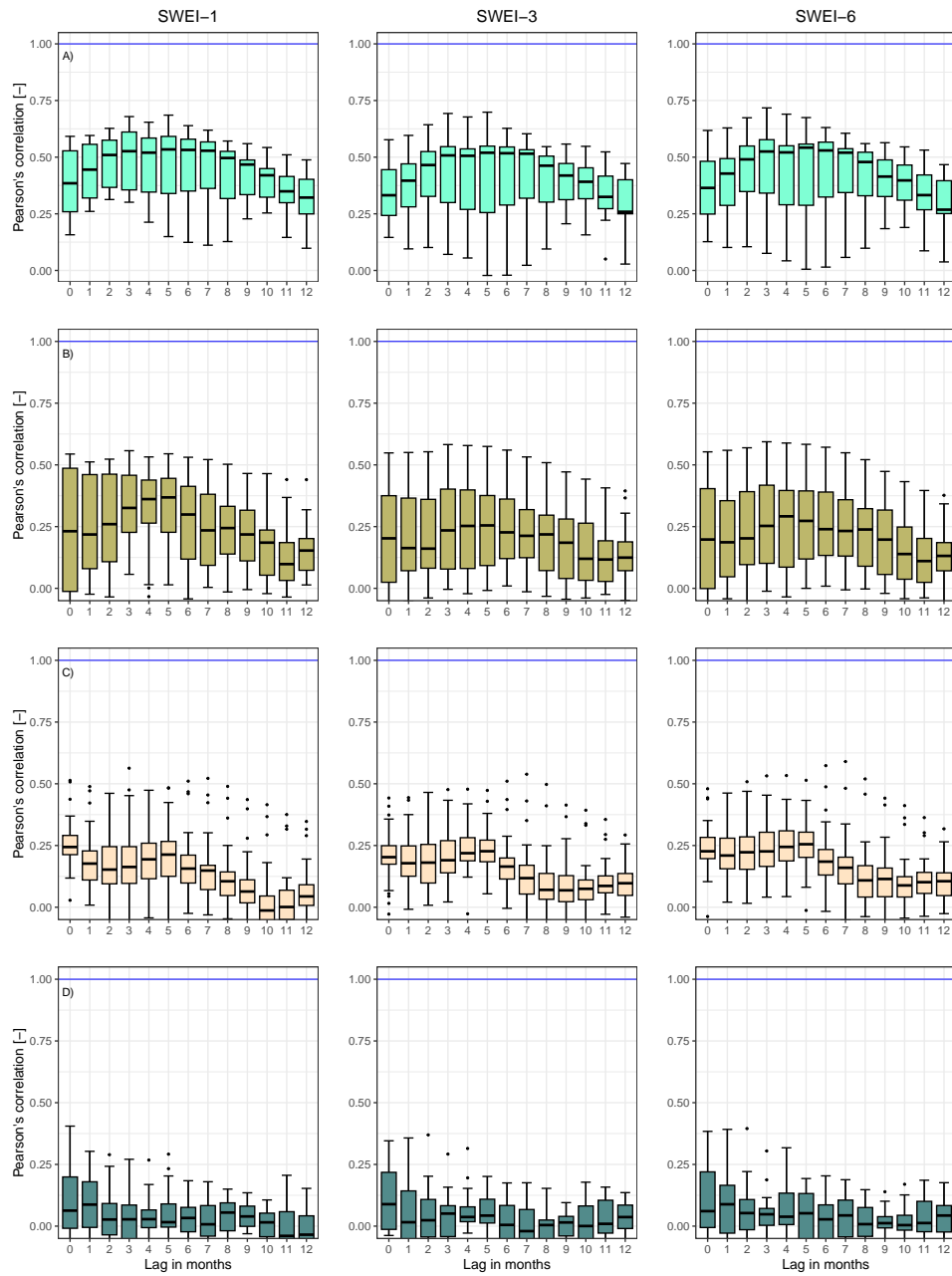


Figure S24. cross-correlation results of the SWEI and the SSI-1 at different lag periods (ranging from 0 to 12 months) for *i*) snow-dominated catchments (a); *ii*) nivo-pluvial (b); *iii*) pluvio-nival (c); and *iv*) rain-dominated (d) catchments. The blue line indicates the optimal cross-correlation. The solid line within each box represents the median value, the edges of the boxes represent the first and third quartiles, and the whiskers extend to the most extreme data point which is no more than 1.5 times the interquartile range from the box.

6. Event coincidence analysis – Hydrological Regimes

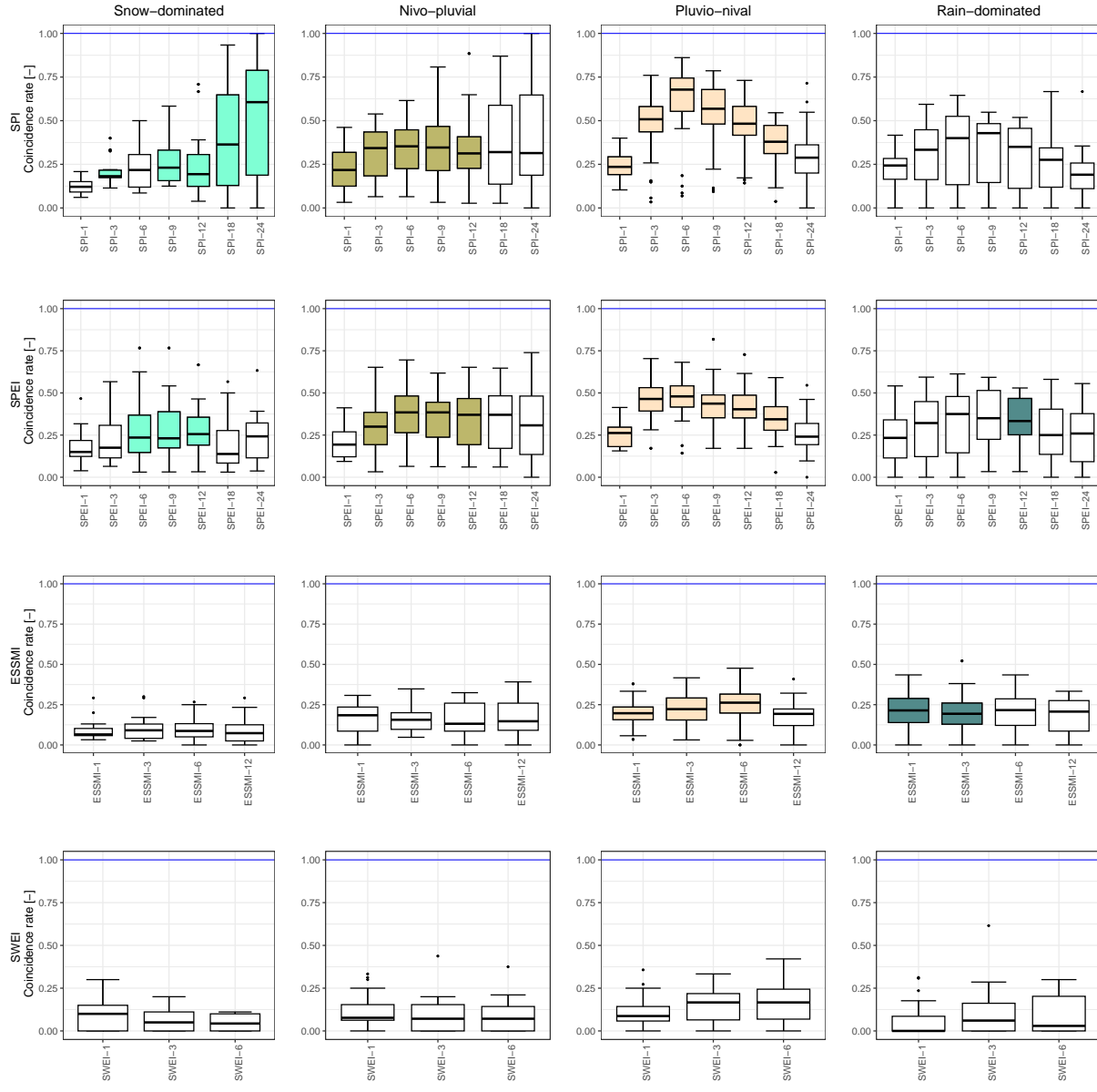


Figure S25. Event coincidence analysis results of the selected drought indices and the SSI-1 for severe droughts at a lag of zero months for *i*) nival; *ii*) nivo-pluvial; *iii*) pluvio-nival; and *iv*) pluvial catchments. The solid boxplots indicate those lags where at least 75% of the catchments presented significant results at the 95% confidence interval, while the white boxplots indicate the opposite. The blue line indicates the optimal cross-correlation. The solid line within each box represents the median value, the edges of the boxes represent the first and third quartiles, and the whiskers extend to the most extreme data point which is no more than 1.5 times the interquartile range from the box.

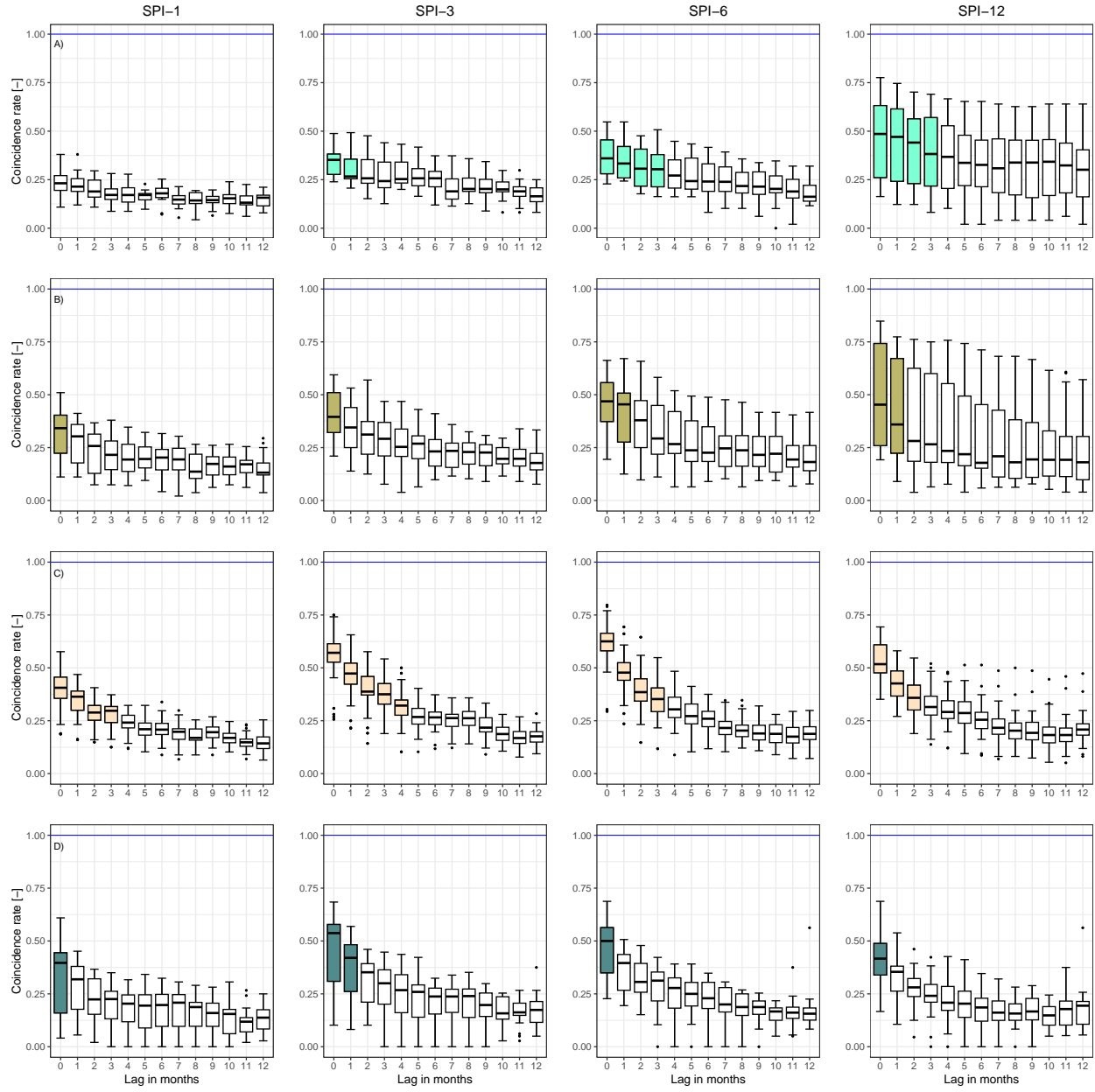


Figure S26. Event coincidence analysis results of the SPI and the SSI-1 for moderate droughts at different lag periods (ranging from 0 to 12 months) for *i*) snow-dominated (a); *ii*) nivo-pluvial (b); *iii*) pluvio-nival (c); and *iv*) rain-dominated (d) catchments. The solid coloured boxplots indicate those lags where at least 75% of the catchments presented significant results at the 95% confidence interval, while the white boxplots indicate the opposite. The blue line indicates the optimal cross-correlation. The solid line within each box represents the median value, the edges of the boxes represent the first and third quartiles, and the whiskers extend to the most extreme data point which is no more than 1.5 times the interquartile range from the box.

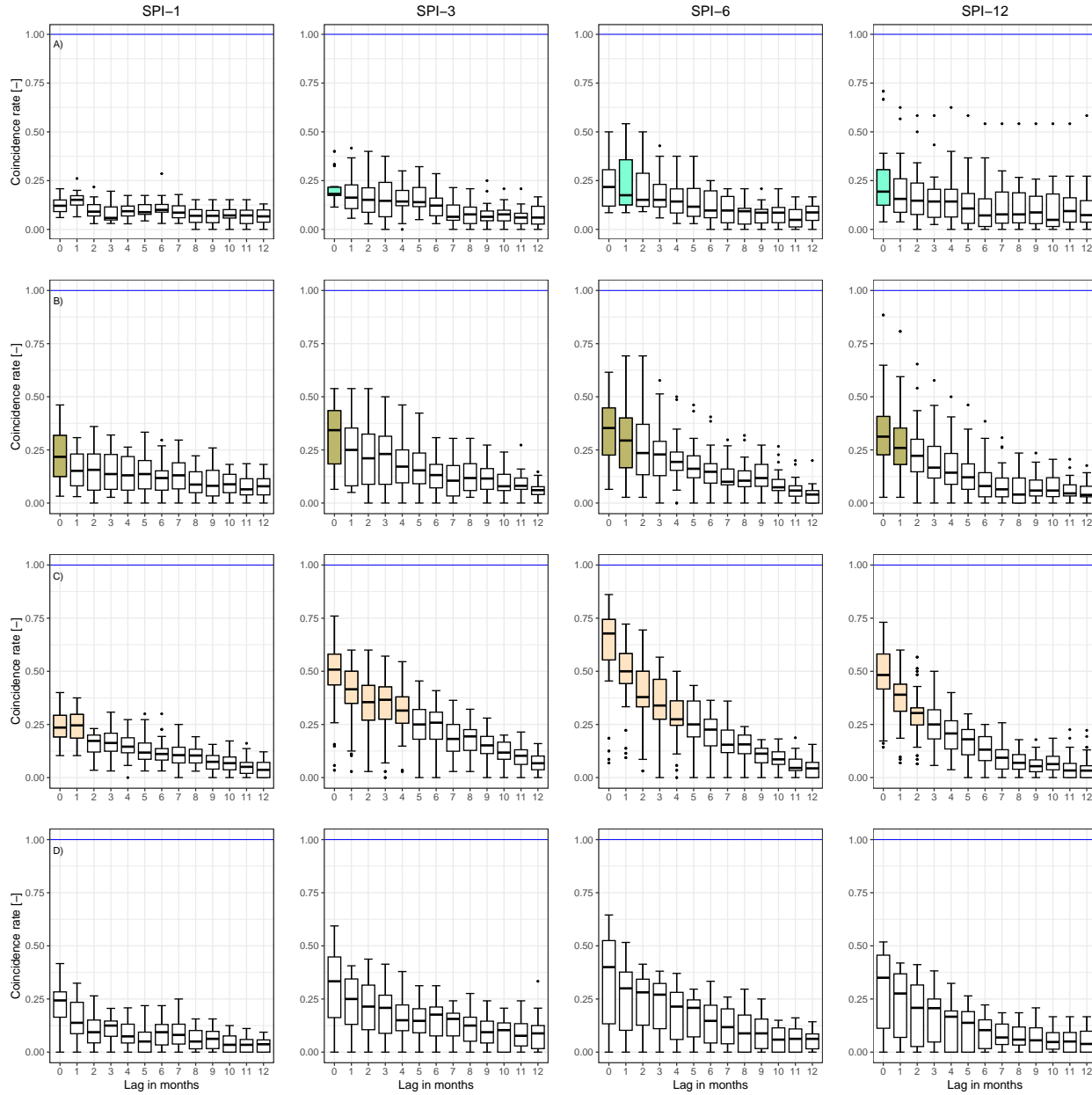


Figure S27. Event coincidence analysis results of the SPI and the SSI-1 for severe droughts at different lag periods (ranging from 0 to 12 months) for *i*) snow-dominated (a); *ii*) nivo-pluvial (b); *iii*) pluvio-nival (c); and *iv*) rain-dominated (d) catchments. The solid coloured boxplots indicate those lags where at least 75% of the catchments presented significant results at the 95% confidence interval, while the white boxplots indicate the opposite. The blue line indicates the optimal cross-correlation. The solid line within each box represents the median value, the edges of the boxes represent the first and third quartiles, and the whiskers extend to the most extreme data point which is no more than 1.5 times the interquartile range from the box.

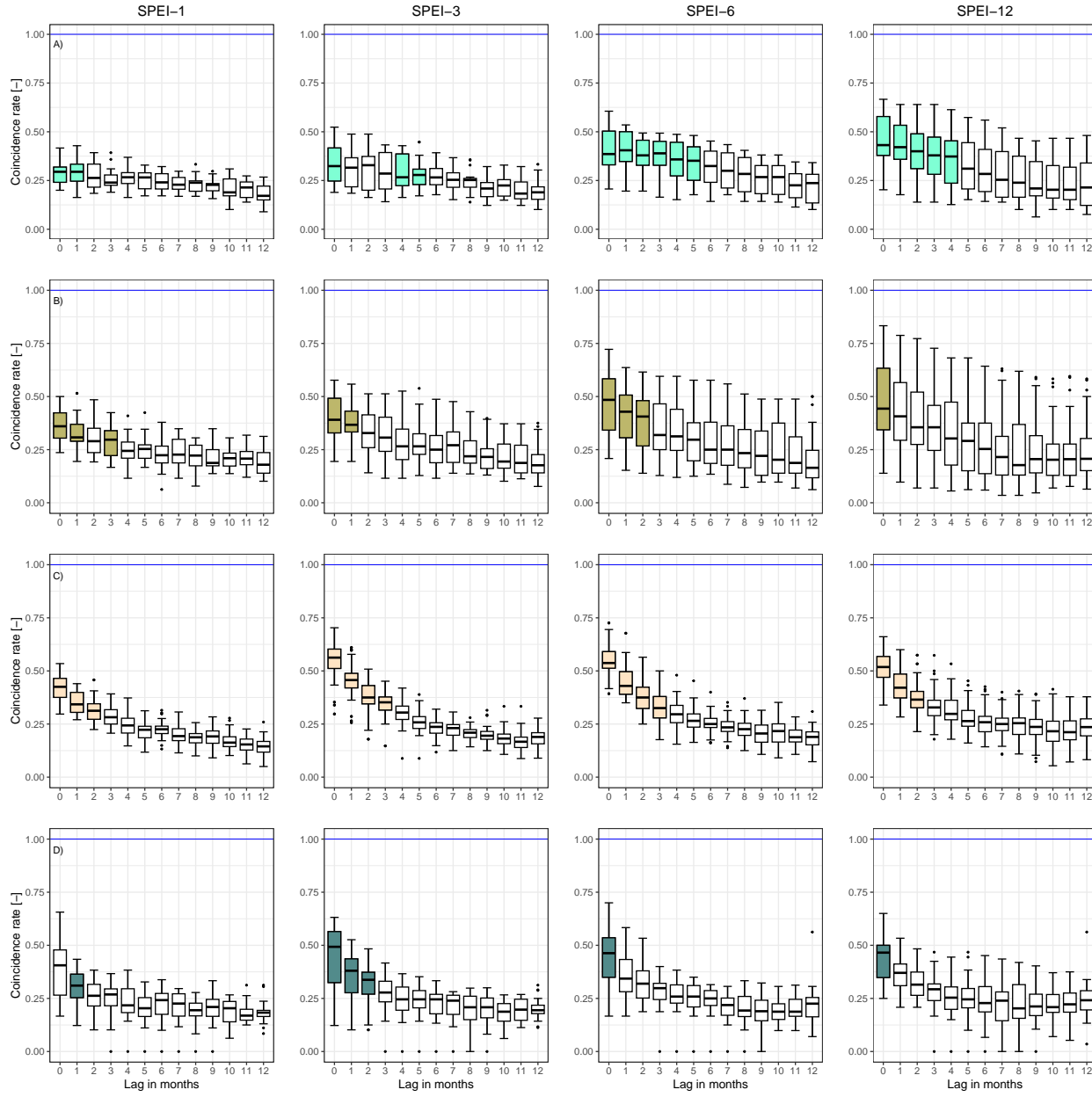


Figure S28. Event coincidence analysis results of the SPEI and the SSI-1 for moderate droughts at different lag periods (ranging from 0 to 12 months) for *i*) snow-dominated (a); *ii*) nivo-pluvial (b); *iii*) pluvio-nival (c); and *iv*) rain-dominated (d) catchments. The solid coloured boxplots indicate those lags where at least 75% of the catchments presented significant results at the 95% confidence interval, while the white boxplots indicate the opposite. The blue line indicates the optimal cross-correlation. The solid line within each box represents the median value, the edges of the boxes represent the first and third quartiles, and the whiskers extend to the most extreme data point which is no more than 1.5 times the interquartile range from the box.

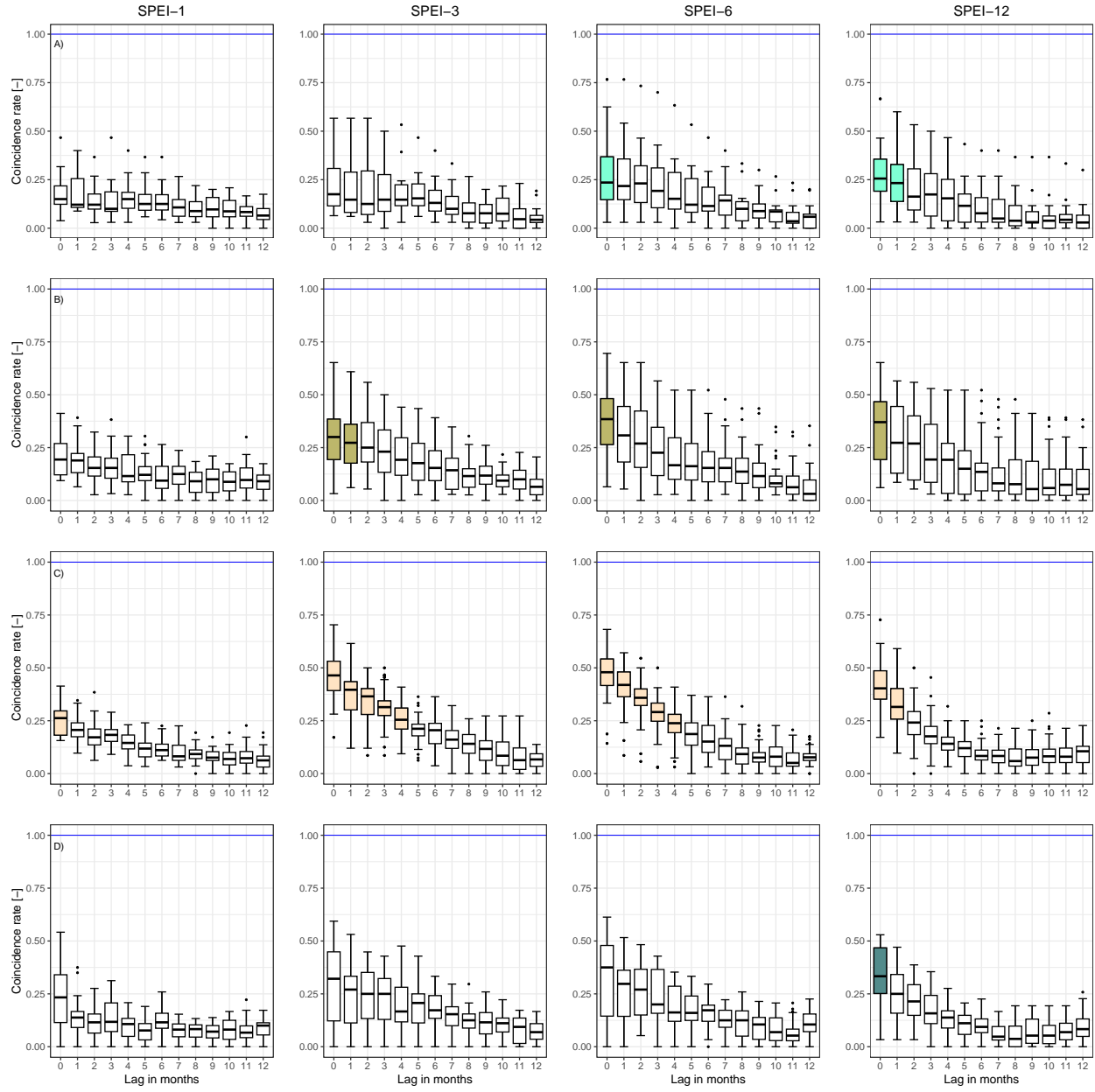


Figure S29. Event coincidence analysis results of the SPEI and the SSI-1 for severe droughts at different lag periods (ranging from 0 to 12 months) for *i*) snow-dominated (a); *ii*) nivo-pluvial (b); *iii*) pluvio-nival (c); and *iv*) rain-dominated (d) catchments. The solid coloured boxplots indicate those lags where at least 75% of the catchments presented significant results at the 95% confidence interval, while the white boxplots indicate the opposite. The blue line indicates the optimal cross-correlation. The solid line within each box represents the median value, the edges of the boxes represent the first and third quartiles, and the whiskers extend to the most extreme data point which is no more than 1.5 times the interquartile range from the box.

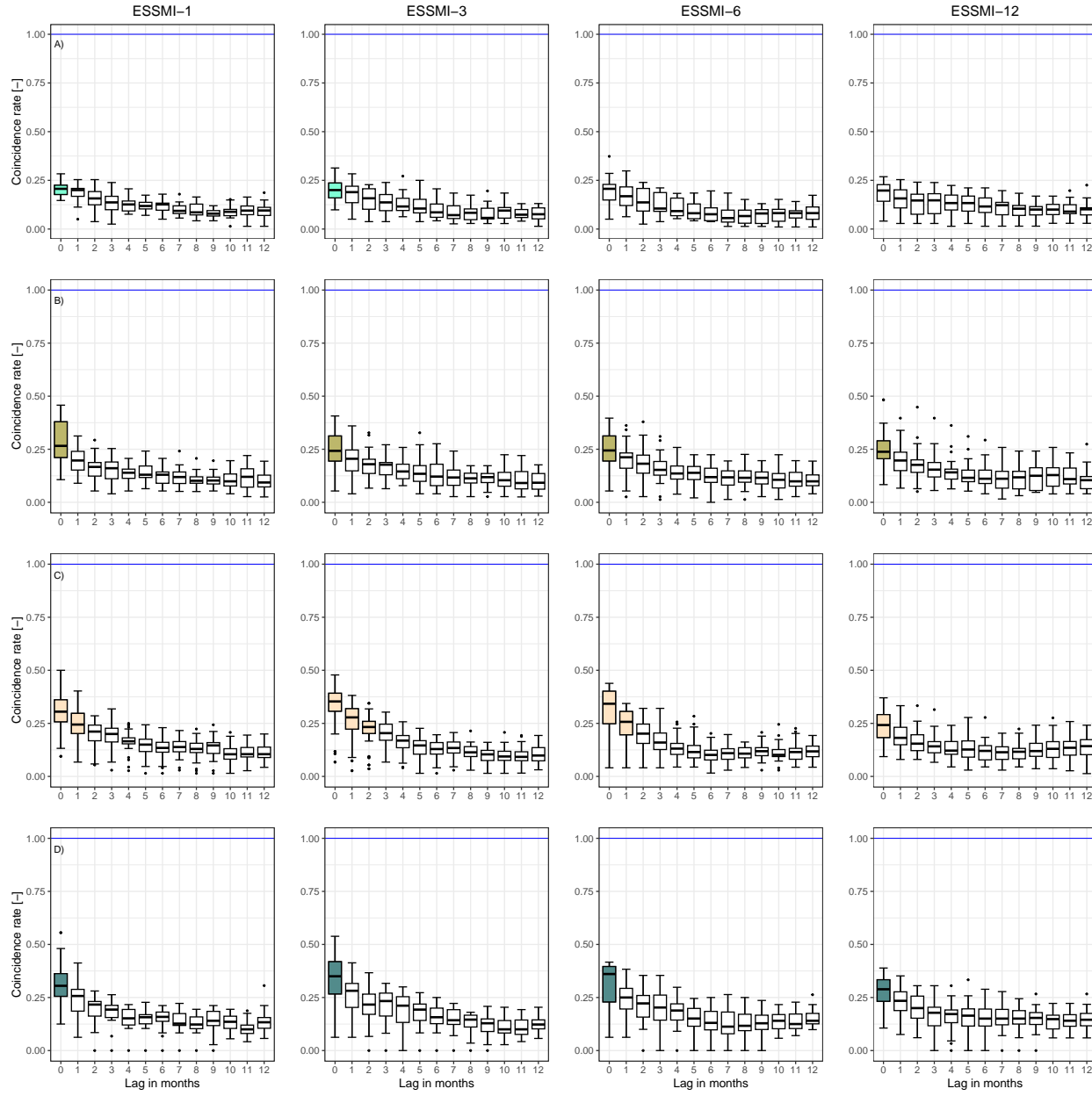


Figure S30. Event coincidence analysis results of the ESSMI and the SSI-1 for moderate droughts at different lag periods (ranging from 0 to 12 months) for *i*) snow-dominated (a); *ii*) nivo-pluvial (b); *iii*) pluvio-nival (c); and *iv*) rain-dominated (d) catchments. The solid coloured boxplots indicate those lags where at least 75% of the catchments presented significant results at the 95% confidence interval, while the white boxplots indicate the opposite. The blue line indicates the optimal cross-correlation. The solid line within each box represents the median value, the edges of the boxes represent the first and third quartiles, and the whiskers extend to the most extreme data point which is no more than 1.5 times the interquartile range from the box. 40

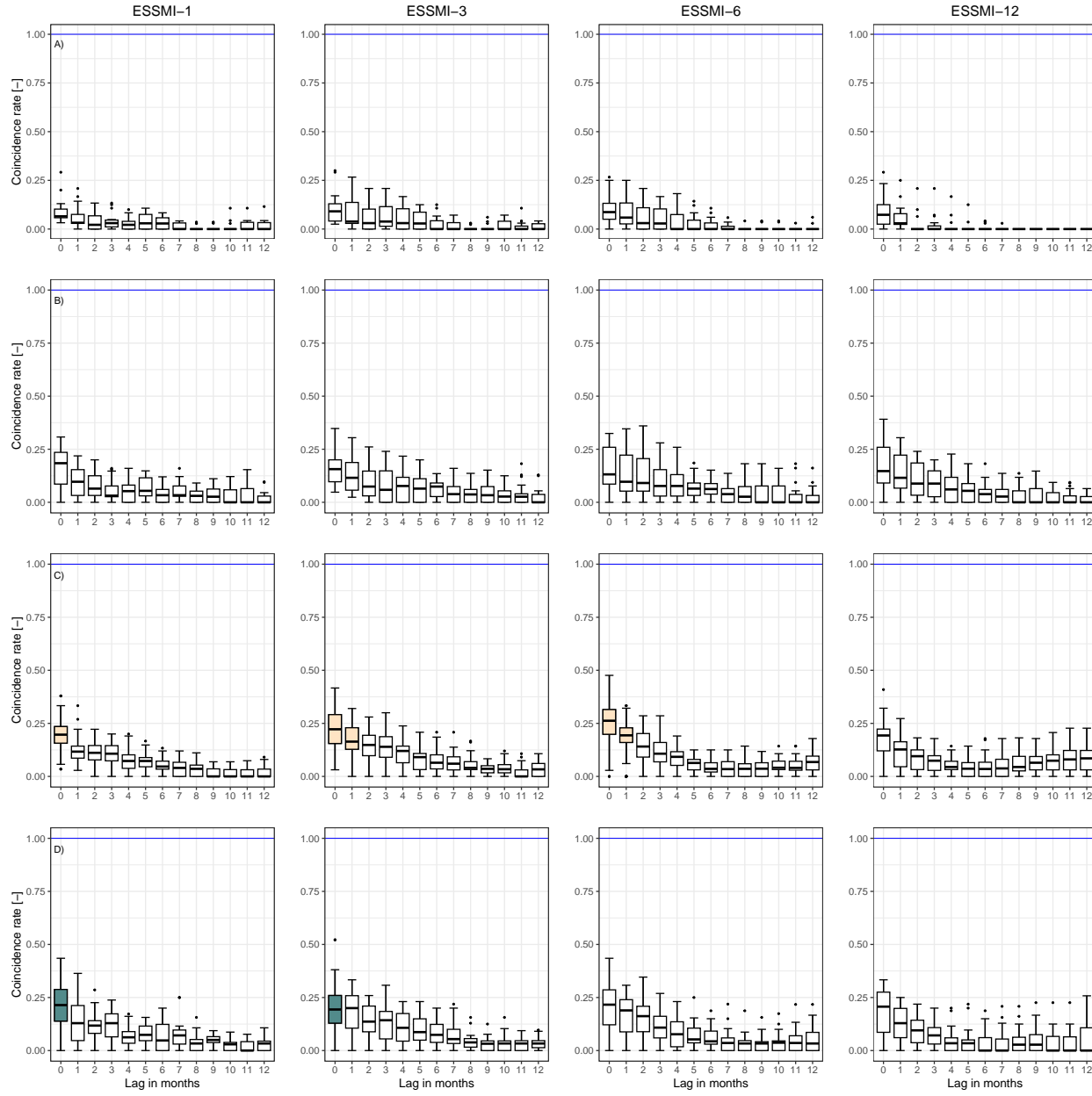


Figure S31. Event coincidence analysis results of the ESSMI and the SSI-1 for severe droughts at different lag periods (ranging from 0 to 12 months) for *i*) snow-dominated (a); *ii*) nivo-pluvial (b); *iii*) pluvio-nival (c); and *iv*) rain-dominated (d) catchments. The solid coloured boxplots indicate those lags where at least 75% of the catchments presented significant results at the 95% confidence interval, while the white boxplots indicate the opposite. The blue line indicates the optimal cross-correlation. The solid line within each box represents the median value, the edges of the boxes represent the first and third quartiles, and the whiskers extend to the most extreme data point which is no more than 1.5 times the interquartile range from the box.

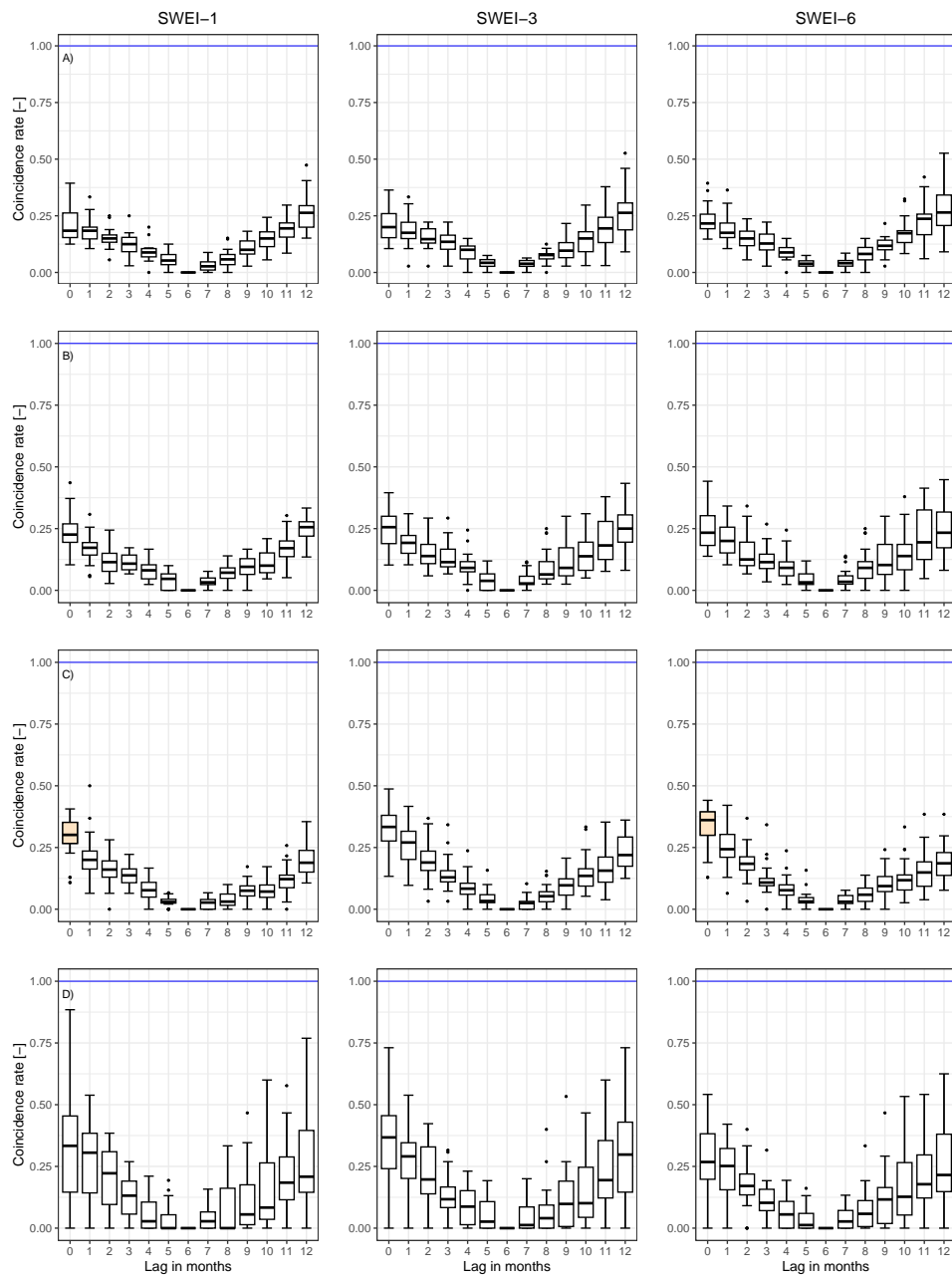


Figure S32. Event coincidence analysis results of the SWEI and the SSI-1 for moderate droughts at different lag periods (ranging from 0 to 12 months) for *i*) snow-dominated (a); *ii*) ~~42~~ pluvio-pluvial (b); *iii*) pluvio-nival (c); and *iv*) rain-dominated (d) catchments. The solid coloured boxplots indicate those lags where at least 75% of the catchments presented significant results at the 95% confidence interval, while the white boxplots indicate the opposite. The blue line indicates the optimal cross-correlation. The solid line within each box represents the median value, the edges of the boxes represent the first and third quartiles, and the whiskers extend to the most extreme data point which is no more than 1.5 times the interquartile range from the box.

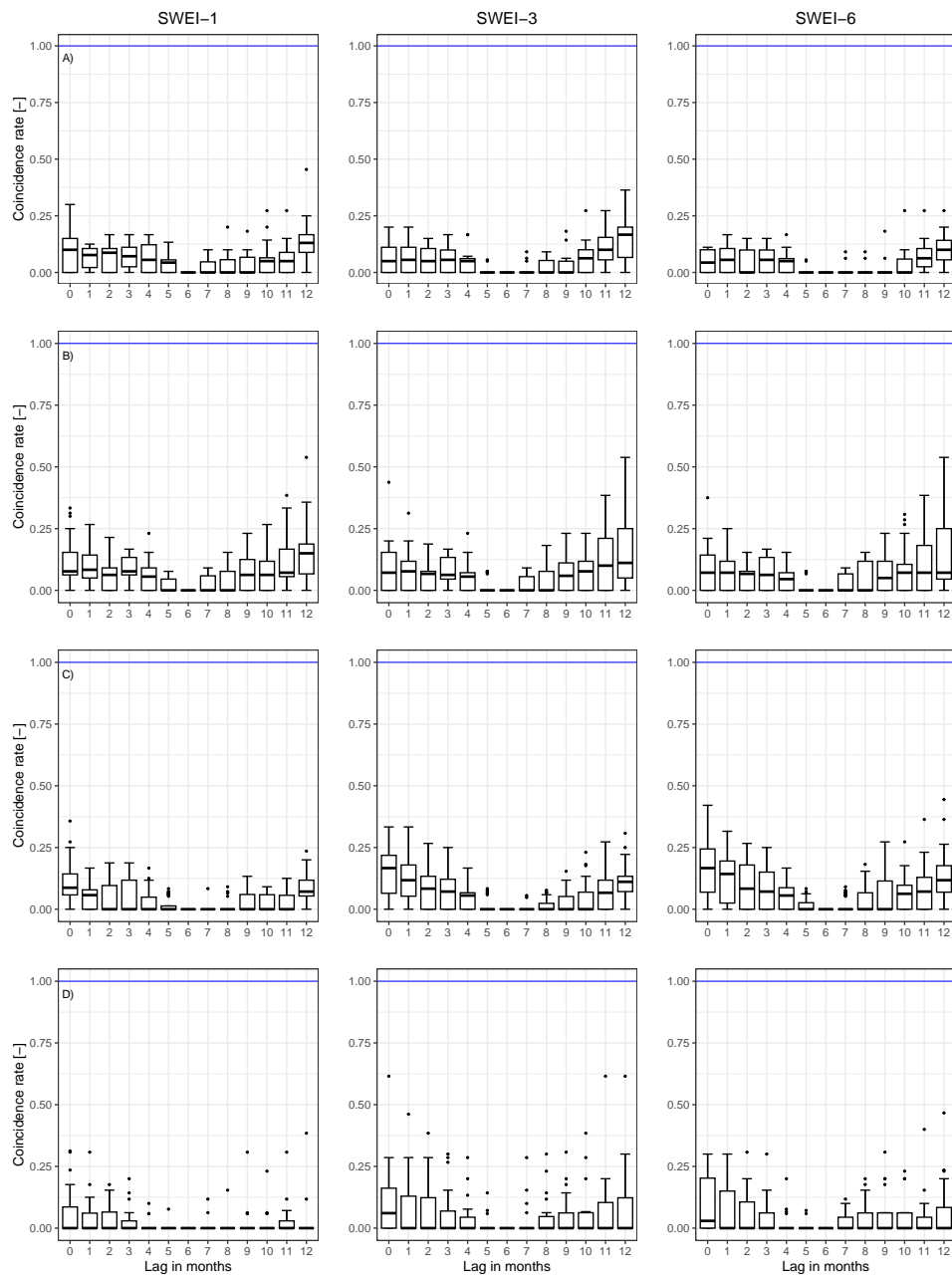


Figure S33. Event coincidence analysis results of the SWEI and the SSI-1 for severe droughts at different lag periods (ranging from 0 to 12 months) for *i*) snow-dominated (a); *ii*) sivo-pluvial (b); *iii*) pluvio-nival (c); and *iv*) rain-dominated (d) catchments. The solid coloured boxplots indicate those lags where at least 75% of the catchments presented significant results at the 95% confidence interval, while the white boxplots indicate the opposite. The blue line indicates the optimal cross-correlation. The solid line within each box represents the median value, the edges of the boxes represent the first and third quartiles, and the whiskers extend to the most extreme data point which is no more than 1.5 times the interquartile range from the box.

7. Catchments with their hydrological regimes

Table S6. Summary of the catchments used in this study with their respective hydrological regimes.

Code	Longitude	Latitude	Regime	Code	Longitude	Latitude	Regime
X01310002	-69.8114	-18.5844	Pluvial	X08304001	-71.2333	-38.4333	Pluvio-nival
X01410004	-69.6669	-18.8269	Pluvial	X09122002	-71.8658	-38.4508	Pluvio-nival
X01730003	-68.9297	-19.8642	Pluvial	X09127001	-72.4167	-38.6167	Pluvio-nival
X02101001	-68.6622	-21.6558	Pluvial	X09129002	-72.5028	-38.6867	Pluvio-nival
X03430003	-69.9747	-28.0003	Nivo-pluvial	X09140001	-72.9469	-38.78	Pluvio-nival
X03414001	-69.9408	-28.0858	Nival	X09134001	-72.3333	-38.85	Pluvio-nival
X04314002	-70.5525	-29.9781	Nival	X09135001	-72.6167	-38.85	Pluvio-nival
X04313001	-70.4344	-30.1222	Nival	X09402001	-71.7336	-38.8653	Pluvio-nival
X04311001	-70.4928	-30.2206	Nival	X09404001	-72.2333	-38.9833	Pluvio-nival
X04501001	-70.5361	-30.4622	Nival	X09437002	-73.0828	-39.0144	Pluvio-nival
X04523002	-70.9244	-30.7047	Nivo-pluvial	X09405001	-72.0833	-39.0333	Pluvio-nival
X04522002	-70.8728	-30.7081	Pluvio-nival	X09434001	-72.6833	-39.1	Pluvio-nival
X04520001	-70.4389	-30.7436	Nival	X09433001	-72.6667	-39.15	Pluvio-nival
X04514001	-70.6128	-30.8128	Nival	X09416001	-71.8244	-39.2561	Pluvio-nival
X04515002	-70.7694	-30.8422	Pluvio-nival	X09420001	-72.2333	-39.2667	Pluvio-nival
X04513001	-70.7731	-30.9242	Nival	X09414001	-71.7667	-39.3333	Pluvio-nival
X04511002	-70.5811	-31.0117	Nival	X09412001	-71.5808	-39.36	Pluvio-nival
X04512001	-70.6644	-31.0119	Nival	X10134001	-72.9	-39.55	Pluvial
X04531002	-71.0403	-31.0325	Nivo-pluvial	X10137001	-72.95	-39.6675	Pluvial
X04530001	-70.885	-31.1119	Nivo-pluvial	X10102001	-71.8497	-39.7267	Pluvio-nival
X04533002	-70.9908	-31.2656	Pluvial	X10111001	-72.475	-39.7667	Pluvio-nival
X04712001	-70.7158	-31.6958	Nivo-pluvial	X10121001	-72.825	-39.8583	Pluvial
X04703002	-70.5944	-31.9667	Nival	X10304001	-72.2667	-40.25	Pluvio-nival
X05101001	-70.7564	-32.0708	Nivo-pluvial	X10306001	-72.2333	-40.2667	Pluvio-nival
X05100001	-70.7119	-32.2253	Nivo-pluvial	X10328001	-73.0022	-40.3842	Pluvio-nival
X05200001	-70.7381	-32.33	Nivo-pluvial	X10364001	-73.2833	-40.5167	Pluvial
X05411001	-70.5403	-32.9164	Pluvio-nival	X10362001	-73.0594	-40.6181	Pluvial
X05721001	-70.3636	-33.3414	Nival	X10356001	-73.2278	-40.7136	Pluvial
X06027001	-70.8739	-34.6867	Nivo-pluvial	X10363002	-73.1333	-40.8856	Pluvial
X07103001	-70.8094	-34.9983	Nivo-pluvial	X10343001	-72.7	-40.9333	Pluvial
X07116001	-71.0911	-35.1731	Pluvial	X10411002	-73.0667	-41.3833	Pluvial
X07372001	-71.3847	-35.1783	Pluvial	X11141001	-71.5478	-44.5936	Nivo-pluvial
X07115001	-71.0156	-35.2744	Nivo-pluvial	X11143001	-71.8083	-44.6592	Nivo-pluvial
X07112001	-71.0028	-35.2783	Nivo-pluvial	X11143002	-72.7167	-44.75	Nivo-pluvial
X07374001	-71.2933	-35.4856	Pluvio-nival	X11302001	-72.1167	-45.15	Nivo-pluvial
X07354002	-71.4419	-36.0028	Pluvio-nival	X11307001	-72.2333	-45.2333	Nivo-pluvial
X07350003	-71.3375	-36.2558	Pluvio-nival	X11308001	-72.4667	-45.3833	Nivo-pluvial
X07330001	-71.6233	-36.3758	Pluvio-nival	X12284003	-72.4833	-51.0167	Nival
X08117005	-72.3167	-36.6167	Pluvio-nival	X12284002	-72.4833	-51.0167	Nival
X08135002	-72.45	-36.65	Pluvio-nival	X12284006	-72.5169	-51.0508	Nival
X08104001	-71.2739	-36.6653	Nivo-pluvial	X12284007	-72.5167	-51.25	Nival
X08132001	-72.3333	-36.8667	Pluvio-nival	X12285001	-72.4667	-51.45	Pluvio-nival
X08130002	-71.5756	-36.9244	Pluvio-nival	X12600001	-71.9414	-52.03	Nivo-pluvial
X08124002	-72.1833	-37.0667	Pluvio-nival	X12452001	-71.9747	-52.5492	Nivo-pluvial
X08123001	-72.0667	-37.15	Pluvial	X12802001	-69.2772	-52.7681	Pluvial
X08334001	-72.5903	-37.5503	Pluvio-nival	X12805001	-69.7536	-52.8497	Pluvial
X08317001	-71.9017	-37.7106	Pluvio-nival	X12586001	-70.9875	-53.1381	Nivo-pluvial
X08342001	-72.3833	-37.85	Pluvio-nival	X12585001	-70.9789	-53.2789	Nivo-pluvial
X08351001	-72.4361	-37.9647	Pluvio-nival	X12582001	-70.9667	-53.65	Nivo-pluvial
X09123001	-72.0106	-38.4303	Pluvio-nival	X12876001	-68.8844	-53.8928	Nivo-pluvial

References

- Baez-Villanueva, O. M., Zambrano-Bigiarini, M., Mendoza, P. A., McNamara, I., Beck, H. E., Thurner, J., Nauditt, A., Ribbe, L., and Thinh, N. X.: On the selection of precipitation products for the regionalisation of hydrological model parameters, *Hydrology and Earth System Sciences*, 25, 5805–5837, 2021.
- Beck, H. E., Van Dijk, A. I., Levizzani, V., Schellekens, J., Miralles, D. G., Martens, B., and Roo, A. d.: MSWEP: 3-hourly 0.25 global gridded precipitation (1979–2015) by merging gauge, satellite, and reanalysis data, *Hydrology and Earth System Sciences*, 21, 589–615, 2017.
- Beck, H. E., Pan, M., Miralles, D. G., Reichle, R. H., Dorigo, W. A., Hahn, S., Sheffield, J., Karthikeyan, L., Balsamo, G., Parinussa, R. M., et al.: Evaluation of 18 satellite-and model-based soil moisture products using in situ measurements from 826 sensors, *Hydrology and Earth System Sciences*, 25, 17–40, 2021.
- Chan, S. K., Bindlish, R., O'Neill, P. E., Njoku, E., Jackson, T., Colliander, A., Chen, F., Burgin, M., Dunbar, S., Piepmeier, J., et al.: Assessment of the SMAP passive soil moisture product, *IEEE Transactions on Geoscience and Remote Sensing*, 54, 4994–5007, 2016.
- Entekhabi, D., Njoku, E. G., O'Neill, P. E., Kellogg, K. H., Crow, W. T., Edelstein, W. N., Entin, J. K., Goodman, S. D., Jackson, T. J., Johnson, J., et al.: The soil moisture active passive (SMAP) mission, *Proceedings of the IEEE*, 98, 704–716, 2010.
- Entekhabi, D., Yueh, S., O'Neill, P. E., Kellogg, K. H., Allen, A., Bindlish, R., Brown, M., Chan, S., Colliander, A., Crow, W. T., et al.: SMAP handbook—soil moisture active passive: Mapping soil moisture and freeze/thaw from space, 2014.
- Hersbach, H., Bell, B., Berrisford, P., Hirahara, S., Horányi, A., Muñoz-Sabater, J., Nicolas, J., Peubey, C., Radu, R., Schepers, D., et al.: The ERA5 global reanalysis, *Quarterly Journal of the Royal Meteorological Society*, 146, 1999–2049, 2020.
- Mohammed, P. N., Aksoy, M., Piepmeier, J. R., Johnson, J. T., and Bringer, A.: SMAP L-band microwave radiometer: RFI mitigation prelaunch analysis and first year on-orbit observations, *IEEE Transactions on Geoscience and Remote Sensing*, 54, 6035–6047, 2016.
- Muñoz-Sabater, J., Dutra, E., Agustí-Panareda, A., Albergel, C., Arduini, G., Balsamo, G., Boussetta, S., Choulga, M., Harrigan, S., Hersbach, H., et al.: ERA5-Land: A state-of-the-art global reanalysis dataset for land applications, *Earth System Science Data*, 13, 4349–4383, 2021.
- Oliva, R., Daganzo, E., Kerr, Y. H., Mecklenburg, S., Nieto, S., Richaume, P., and Gruhier, C.: SMOS radio frequency interference scenario: Status and actions taken to improve the RFI environment in the 1400–1427-MHz passive band, *IEEE Transactions on Geoscience and Remote Sensing*, 50, 1427–1439, 2012.
- O'Neill, P., Chan, S., Njoku, E., Jackson, T., Bindlish, R., and Chaubell, J.: SMAP enhanced L3 radiometer global daily 9 km EASE-grid soil moisture, version 3, NASA National Snow and Ice Data Center Distributed Active Archive Center, Boulder, Colorado USA, 2016.
- Reichle, R., De Lannoy, G., Koster, R. D., Crow, W. T., Kimball, J. S., and Liu, Q.: SMAP L4 global 3-hourly 9 km EASE-grid surface and root zone soil moisture geophysical data, version 4, NASA National Snow and Ice data center distributed active archive center, 10, 2018.
- Tavakol, A., Rahmani, V., Quiring, S. M., and Kumar, S. V.: Evaluation analysis of NASA SMAP L3 and L4 and SPoRT-LIS soil moisture data in the United States, *Remote Sensing of Environment*, 229, 234–246, 2019.